

Demonstrating anyonic non-Abelian statistics with a minimal $d = 6$ qudit lattice

Lucy Byles,* Ewan Forbes, and Jiannis K. Pachos

School of Physics and Astronomy, University of Leeds, Leeds, LS2 9JT, United Kingdom

(Dated: March 12, 2025)

Quantum double models provide a natural framework for realising anyons by manipulating a lattice of qudits, which can be directly encoded in quantum simulators. In this work, we consider a lattice of $d = 6$ qudits that give rise to $\mathbf{D}(\mathbf{S}_3)$ non-Abelian anyons. We present a method that demonstrates the non-commutativity of the braiding and fusion evolutions solely by utilising the operators that create and measure anyons. Furthermore, we provide a dense coding scheme where only two qudits are sufficient to determine the anyonic braiding and fusion matrices. The minimal resource requirement of our approach offers a viable blueprint for demonstrating the non-Abelian nature of anyons in various quantum platforms, including optical, atomic, and solid-state systems, where higher-spin states can be effectively encoded. This work represents a foundational step towards the realisation of non-Abelian quantum error-correcting codes.

I. INTRODUCTION

Anyons introduced a surprising shift in the paradigm of quantum computation when it was shown that these quasiparticles with exotic statistics could be implemented as a means to perform fault-tolerant quantum evolutions [1–3]. As long as anyons remain intact, the quantum information encoded in them remains protected from destructive environmental perturbations. Soon anyonic quantum computation gave rise to a host of potential benefits for quantum information, such as the discovery of a new quantum algorithm for the efficient evaluation of Jones polynomials [4] and the proposal of new methods to combat thermal errors [5–11]. Furthermore, anyonic systems can be directly translated into quantum error-correcting codes with high error thresholds and minimal resource requirements [12, 13].

The potential applications of anyons to quantum computation have sparked a race for their physical realisation. Fractional quantum Hall liquids [14–17] and topological superconductors [18–21] are the most promising platforms for the realisation of non-Abelian anyons capable of manipulating quantum information in a non-trivial way. Nevertheless, these platforms are highly complex, exhibiting a richness of physical effects [22]. Moreover, anyons by their nature hide information rather well from the environment as well as from experimentalists. Hence, it is rather challenging to identify the non-Abelian statistics of anyons in a physical system. To overcome some of these complexities, a significant effort has been dedicated in the physical simulation of quantum systems that give rise to certain properties of anyons [23–27]. Such quantum simulations allow for the effective isolation of

the statistical properties of anyons from other physical effects, providing a platform to conclusively observe signatures of their non-Abelian behaviour.

Here, we focus on a particular aspect of non-Abelian anyons, namely the non-commutativity of their topological evolutions. This non-commutativity is manifested in various quantum states when braiding non-Abelian anyons in different combinations. At an elementary level this is encoded in the non-commutativity of the braiding, R , and fusion recombination, F , evolutions of non-Abelian anyons. Physically, this dictates that recombining anyons in a different fusion order after a braiding evolution changes the resulting state in a non-trivial way. This fundamental property gives rise to a host of signatures of non-Abelian anyonic systems, such as the restricted multiplicity in their ground state degeneracy recently observed experimentally [28].

In principle, the braiding and fusion evolutions require the transport of anyons. When implemented in a quantum simulation, transport of non-Abelian anyons requires complex controlled evolutions that achieves their transport without read-out of their encoded information. To bypass the requirement of such complex operations, we devise a static method of obtaining the R and F evolutions by employing projective measurements in anyonic bases, thus significantly simplifying the required experimental resources. Similar approaches using measurements to circumvent the need for anyonic transportation have been seen previously in [29, 30].

For concreteness, we consider one of the simplest quantum double models, namely the $\mathbf{D}(\mathbf{S}_3)$ anyonic model, that supports non-Abelian anyons [2]. This quantum double model is supported on a square lattice of $d = 6$ qudits. The vacuum of the system corresponds to the ground state of a particular Hamiltonian consisting of

* pylsb@leeds.ac.uk

local plaquette and vertex projectors. Pairs of anyons are generated at the endpoints of strings or ribbons of operations acting on the qudits [31–33]. We demonstrate non-Abelianity by considering only static anyonic configurations, i.e. generating anyons and applying projective measurements without the need to move any non-Abelian anyons. Moreover, we show how to determine the R and F matrices by employing the minimal resources of two qudits, thus greatly simplifying the experimental requirements. Similar investigations of non-Abelian anyons supported by the Fibonacci string-net model have been recently contacted in [34–36]. These require larger systems and more complex manipulations, but with the added advantage of supporting a universal set of topological operations. We envision that the quantum simulation seen here can be directly realised with various quantum technology platforms, ranging from photonic systems [37–39] to Rydberg atoms [40, 41]. Such experimentally accessible quantum simulations offer a direct approach for realising anyonic statistics in the laboratory (see Appendix A).

This paper is organised as following. In Section II we present the main elements of the $\mathbf{D}(\mathbf{S}_3)$ quantum double model and a specific subset of non-Abelian anyons it supports. A minimal set of steps that determine the R matrix are given in Section III, while a simple method that determines the fusion recombination F matrix is given in Section IV. In Section V we provide a dense coding of the system where only two $d = 6$ qudits are needed to demonstrate the non-Abelian character of the $\mathbf{D}(\mathbf{S}_3)$ anyons. Finally, Section VI provides concluding remarks and outlook.

II. THE $\mathbf{D}(\mathbf{S}_3)$ QUANTUM DOUBLE MODEL

The use of quantum double models for topological quantum computation was first proposed by Alexei Kitaev in his seminal 2003 paper [2]. Such models describe a generalised code defined on a lattice of qudits with spin levels labelled by the elements of a chosen finite group, \mathbf{G} . The group \mathbf{G} defines the algebraic structure of the quantum double $\mathbf{D}(\mathbf{G})$, dictating the anyons present and their associated fusion and braiding relations.

Here, we provide a brief overview (expanded upon in Appendix C) of the properties we make use of in $\mathbf{D}(\mathbf{S}_3)$, the simplest quantum double model that can support non-Abelian anyons. This model describes eight distinct types of anyon, labelled $\{A, B, C, D, E, F, G, H\}$, corresponding to each of the eight irreducible representations of the quantum double of \mathbf{S}_3 [33, 42]. Instead of considering the complete set of eight anyons, it is instructive to

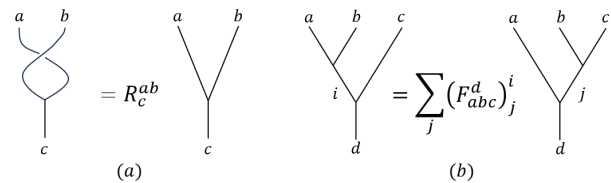


FIG. 1. The R and F operations that characterise anyonic models. (a) The R braid describes the phase, R_c^{ab} , gained by exchanging two anyons, a and b when they have a fixed fusion outcome c . (b) The $(F_{abc}^d)_j^i$ matrix elements give the relation between the states of three fusing anyons a , b , and c with fixed fusion outcome d when the order of fusion is changed.

restrict to a smaller sub-group of this model that is closed under fusion. In this way, the non-Abelian properties can be demonstrated, while reducing the complexity of theoretical and experimental treatment. Here we will consider the sub-group $\{A, B, G\}$ where A is the vacuum, B is an Abelian anyon and G is a non-Abelian anyon. Their fusion relations are given by

$$\begin{aligned} A \times A &= B \times B = A, \\ G \times B &= G, \\ G \times G &= A + B + G. \end{aligned} \quad (1)$$

The fusion multiplicity of the G anyon signals its non-Abelian nature such that the fusion space of a pair of G anyons forms a multi-dimensional Hilbert space spanned by a set of anyonic basis states $|G, G \rightarrow i\rangle$ where $G, G \rightarrow i$ indicates the fusion of two G anyons to outcome $i = A, B, G$. To demonstrate the non-triviality of the braiding of these anyons we start by introducing the F and R matrices, the basic operations for the manipulation of anyons. The goal of this paper is to present a method in which these matrices can be reproduced with local operations on a lattice, thus explicitly demonstrating the non-Abelianity of the G anyons in the $\mathbf{D}(\mathbf{S}_3)$ quantum double model.

A. The R and F Matrices

The R matrix dictates the change in phase gained when two anyons undergo a counter-clockwise exchange, given as

$$R_{\circlearrowleft} |a, b \rightarrow c\rangle = R_c^{ab} |a, b \rightarrow c\rangle, \quad (2)$$

for two anyons a and b fusing to an anyon c , where R_{\circlearrowleft} corresponds to the anti-clockwise exchange of a and b anyons, as shown in Figure 1(a). For the non-Abelian fusion of two G anyons, the fusion multiplicity generates a 3×3 diagonal unitary matrix R^{GG} with entries

$(R^{GG})_i^i \equiv R_i^{GG}$, the form of which may be analytically determined using a set of self-consistent relations known as the pentagon and hexagon relations [43]. The matrix R^{GG} is found to take the form

$$R^{GG} = \begin{pmatrix} \omega & 0 & 0 \\ 0 & -\omega & 0 \\ 0 & 0 & \bar{\omega} \end{pmatrix}, \quad (3)$$

with $\omega = e^{\frac{2\pi i}{3}}$ and $\bar{\omega} = \omega^*$.

The fusion matrix describes the mapping between two states of three anyons a, b and c fusing to a final anyon, d , with the order of fusion changed as in Figure 1(b). The action of this mapping may be described in the anyonic basis as

$$|(a, b), c \rightarrow i, c \rightarrow d\rangle = \sum_j (F_{abc}^d)_j^i |a, (b, c) \rightarrow a, j \rightarrow d\rangle. \quad (4)$$

For the fusion of three G anyons to total fusion outcome G , the intermediary anyons i and j may be A, B or G . F_{GGG}^G is therefore a 3×3 matrix, found analytically to take the form

$$F_{GGG}^G = \frac{1}{2} \begin{pmatrix} 1 & 1 & \sqrt{2} \\ 1 & 1 & -\sqrt{2} \\ \sqrt{2} & -\sqrt{2} & 0 \end{pmatrix}. \quad (5)$$

For the basis $\{|(a, b), c \rightarrow i, c \rightarrow d\rangle\}$ the braid group of the three anyons a, b and c is composed of two operations, b_1 and b_2 braiding the pairs (a, b) and (b, c) respectively. For identical anyons $a = b = c = d = X$, it can be shown (see [44]), that these braiding operators can be written in terms of the R and F matrices as $b_1^X = R^{XX}$ and $b_2^X = (F_{XXX}^X)^{-1} R^{XX} F_{XXX}^X$. We note that if $[R^{XX}, F_{XXX}^X] = 0$ then $b_2^X = R^{XX} = b_1^X$. Hence, the braiding operations b_1^X and b_2^X commute and both matrices are diagonal and thus incapable of producing non-trivial unitary transformations of the anyonic Hilbert space. For such systems, all n^{th} order products of b_1^X and b_2^X will simply act to produce phases on the anyonic basis states. The R and F matrices therefore encode the description of the braiding matrices underpinning the power of such anyonic models for performing non-trivial quantum computation [3].

For the G anyons of the $\{A, B, G\}$ subgroup, b_2^G is a non-diagonal matrix describing a non-trivial unitary evolution of the basis $\{|(G, G), G \rightarrow i, G \rightarrow G\rangle\}$. Furthermore, it has been shown that the square of this operation

$$(b_2^G)^2 = (F_{GGG}^G)^{-1} (R^{GG})^2 F_{GGG}^G, \quad (6)$$

$$= \begin{pmatrix} \cos \frac{2\pi}{3} & -i \sin \frac{2\pi}{3} & 0 \\ -i \sin \frac{2\pi}{3} & \cos \frac{2\pi}{3} & 0 \\ 0 & 0 & \bar{\omega} \end{pmatrix}, \quad (7)$$

can be used in the generation of valuable non-stabilizer magic states [45], crucial for the development of universal computational schemes [46, 47]. Note that $(b_1^G)^2$ and $(b_2^G)^2$ are non-commuting braidings resulting from the non-commutativity of the $(R^{GG})^2$ and F_{GGG}^G matrices. In contrast, the non-Abelian anyon, C , of the charge subgroup $\{A, B, C\}$, has an R matrix of the form

$$R^{CC} = \begin{pmatrix} 1 & 0 & 0 \\ 0 & -1 & 0 \\ 0 & 0 & 1 \end{pmatrix}, \quad (8)$$

such that $(b_1^C)^2 = (b_2^C)^2 = \mathbf{1}_3$. Hence, these processes commute, limiting the comparative capability of such a model to perform non-trivial computation [48].

B. Anyonic manipulation on a lattice

We now present the lattice model that gives rise to the quantum double $\mathbf{D}(\mathbf{S}_3)$ presented above. Consider a two-dimensional square lattice with orientation as shown in Figure 2. On each link of the lattice a Hilbert space, \mathbf{H} , described by $d = 6$ qudits ($\dim(\mathbf{H}) = 6$) is placed with orthonormal basis indexed by the group elements of \mathbf{S}_3 , $\{|g\rangle : g \in \mathbf{S}_3\}$

The dynamics of our model are given by the Kitaev Hamiltonian [2]

$$\mathcal{H} = - \sum_v A(v) - \sum_p B(p), \quad (9)$$

for vertex and plaquette operators $A(v)$ and $B(p)$ respectively as shown in Figure 2(b), defined on a lattice with open boundaries, producing a unique ground state $|\zeta\rangle$, corresponding to the anyonic vacuum, in which

$$A(v)|\zeta\rangle = |\zeta\rangle, \quad B(p)|\zeta\rangle = |\zeta\rangle, \quad (10)$$

for all vertices, v , and plaquettes, p . Excitations of this model are particle-like and are indicated by violations of the conditions (10). Fluxons (chargeons) are anyonic excitations with non-trivial flux (charge) positioned on the plaquette (vertex) of the lattice for which $B(p)|\zeta\rangle \neq |\zeta\rangle$ ($A(v)|\zeta\rangle \neq |\zeta\rangle$). This model also admits the description of dyons— composite particles defined on a neighbouring vertex and plaquette.

The anyons in our reduced model $\{A, B, G\}$ may be coherently created and manipulated with the application of so-called ribbon operators to this anyonic ground state. The A and B anyons are both Abelian with trivial flux, and can therefore be created and moved with string operators corresponding to paths on the direct lattice. As A is the vacuum particle, the operator F^A acts trivially

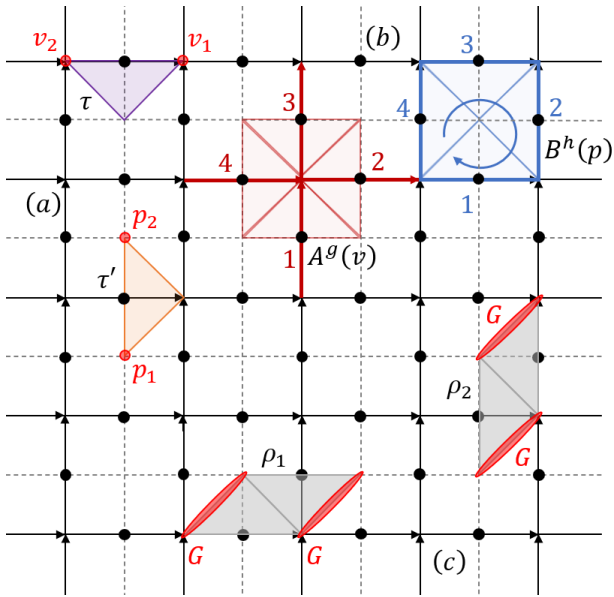


FIG. 2. The lattice construction of the quantum double model $\mathbf{D}(\mathbf{S}_3)$. The solid lines denote the direct lattice with underlying orientation as indicated by arrows. The dual lattice is shown with dotted lines. At the top of (a), an example of a direct triangle is shown as outlined in equation (C15). The direct triangle, τ , creates excitations on vertices v_1 and v_2 as shown. Below, is a dual triangle as defined in equation (C14). The dual triangle, τ' , creates a pair of excitations on plaquettes p_1 and p_2 . In (b) closed loops of these dual (direct) triangles form the vertex (plaquette) operators. The orientation of each of the component operators depends on the lattice enumeration and ensures that all $A^g(v)$ and $B^h(p)$ mutually commute. (c) The two G anyonic ribbons ρ_1 and ρ_2 that will be used throughout the paper. The dyons created by the associated ribbon operators $F_{\rho_1}^G$ and $F_{\rho_2}^G$ are situated along the sites formed of the vertices and plaquettes at the endpoints of each ribbon as highlighted.

as the identity matrix. Both A and B anyons may be transported around the lattice similarly to e and m particles in the toric code by applying these single-qudit ribbon operators to strings of qudits. In contrast, the G anyons are dyons that have both non-trivial flux and charge. They therefore require the implementation of ribbon operators composed of dual and direct triangles for their manipulation [49] (see also Appendix B 2). A simple ribbon operator capable of producing a pair of G anyons can be composed of one direct and one dual triangle, $\rho = \tau_{\text{direct}}\tau_{\text{dual}}$. In the following we will consider two distinct two-qudit ribbon operators, $F_{\rho_1}^G$ and $F_{\rho_2}^G$, as illustrated in Figure 2(c). We note that both of these operators are Hermitian but not unitary (see Appendix C 2 for explicit forms of these operators). Nevertheless, when restricted to act on the eigenstates of (9), they return normalised states [31]. These ribbons are sufficient

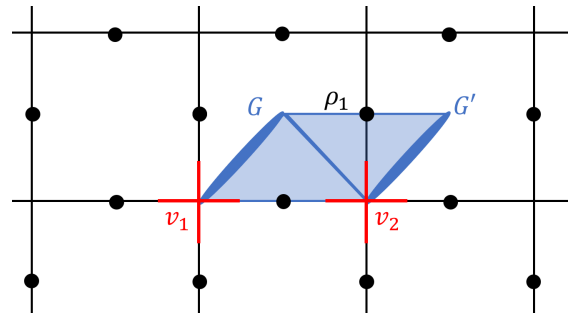


FIG. 3. The anyonic ribbon operator $F_{\rho_1}^G$ creates a pair of dyons G and G' at the endpoints of the ribbon ρ_1 when acting on the ground state $|\zeta\rangle$. In the $\{A, B, G\}$ sub-model, anyons can be measured with the application of the vertex projection operators such as in (11). In this way, the state $F_{\rho_1}^G|\zeta\rangle$ is preserved under the action of the measurement operators $A^G(v_1)$ and $A^G(v_2)$.

to demonstrate the fusion and braiding properties of the G anyons of $\mathbf{D}(\mathbf{S}_3)$, given in (3) and (5), as we shall see in the next sections.

Finally, we will introduce a set of local measurement operators that distinguish between each anyon type. This is particularly useful when we want to determine the fusion outcome of two anyons while constructing anyonic basis states such as $|G, G \rightarrow i\rangle$, with $i = A, B, G$. Locality dictates that when two anyons fuse together to produce some overall particle type then both fusing particles must be measured jointly [44]. The initial anyons may be spatially separated, in which case the fusion outcome measurement must be performed around a loop that surrounds both anyons under fusion. For the operations considered here we ensure that the pair of particles undergoing fusion share a common vertex. In this way each outcome A, B, G can be measured by the respective four-body vertex projection operator $A^{A/B/G}(v)$ as in [42], which project onto the chosen anyon by measuring the charge. These projectors are sufficient in distinguishing between the possible anyonic charges that lay on a chosen vertex v , such that for example for the ground state anyonic vacuum, $|\zeta\rangle$, $A^A(v)|\zeta\rangle = |\zeta\rangle$ and $A^B(v)|\zeta\rangle = A^G(v)|\zeta\rangle = 0$, for all vertices.

In order to further illustrate the action of these vertex operators consider Figure 3. The ribbon $F_{\rho_1}^G$ creates a pair of G dyons with sites lying on vertices v_1 and v_2 . Application of A^G to either vertex will therefore preserve the state, $A^G(v_1)F_{\rho_1}^G|\zeta\rangle = F_{\rho_1}^G|\zeta\rangle$, verifying the creation of a G anyon, while $A^A(v_1)F_{\rho_1}^G|\zeta\rangle = A^B(v_1)F_{\rho_1}^G|\zeta\rangle = 0$ (and similarly for v_2). By employing these projectors on the lattice we can also verify the fusion rules of two G anyons as given in (1). The repeated application of $F_{\rho_1}^G$ produces a pair of G dyons at both v_1 and v_2 . Applying

a vertex projection operator to either vertex therefore measures the fusion of two G anyons at that point. For example, it is found that

$$\begin{aligned} A^A(v_1)(F_{\rho_1}^G)^2|\zeta\rangle &= |\zeta\rangle, \\ A^B(v_1)(F_{\rho_1}^G)^2|\zeta\rangle &= F_{\tau_1}^B|\zeta\rangle, \\ A^G(v_1)(F_{\rho_1}^G)^2|\zeta\rangle &= F_{\rho_1}^G|\zeta\rangle, \end{aligned} \quad (11)$$

where $F_{\tau_1}^B$ is the direct triangle ribbon operator producing a pair of B anyons on vertices v_1 and v_2 , indicating that the fusion of a pair of G anyons gives rise to a superposition of A , B and G anyons as dictated by the fusion rule $G \times G = A + B + G$.

III. R MATRIX DERIVATION

In Section II A we introduced the matrices R^{GG} and F_{GGG}^G , describing the statistical evolutions of the non-Abelian G anyons of the $D(S_3)$ quantum double model. The implementation of these evolutions within the framework of the quantum double was first considered by Kitaev in his foundational work [2]. Here, we begin by presenting such a method by which experimentally accessible ribbon operators may be used to extract the braiding properties of G anyons contained in the matrix elements of $(R^{GG})^2$.

A. R matrix from ribbon operators

Consider the ribbon operators F_{ρ}^a and $F_{\rho'}^b$, creating pairs of anyons (a, \bar{a}) and (b, \bar{b}) respectively as shown in Figure 4. By considering two equivalent sets of operations connecting the products $F_{\rho}^a F_{\rho'}^b$ and $F_{\rho'}^b F_{\rho}^a$ we will show how the elements of the braiding matrix R^{ab} may be extracted from the commutativity of reduced ribbon operators. First, consider exchanging the order of F_{ρ}^a and $F_{\rho'}^b$, as shown in the top line of Figure 4. For all points where the two ribbons do not overlap (indicating action on different qudits on the lattice), such an exchange is trivial. Alternatively, the exchange of these ribbon operators may be interpreted in terms of the projection of the braiding of anyonic worldlines. Both ribbons share common start and end points such that the fusion outcome $a \times b \rightarrow c$ may be fixed with the application of a localised projection operator P^c to the point of overlap of a and b (superselection rules then dictate that $\bar{a} \times \bar{b} \rightarrow \bar{c}$ such that the total system will still fuse to the vacuum). By analogy with Figure 1(a), ‘undoing’ the braiding of the ribbons on the LHS with a clockwise rotation therefore produces any topologically equivalent configuration to that in the centre of Figure 4 with an additional factor

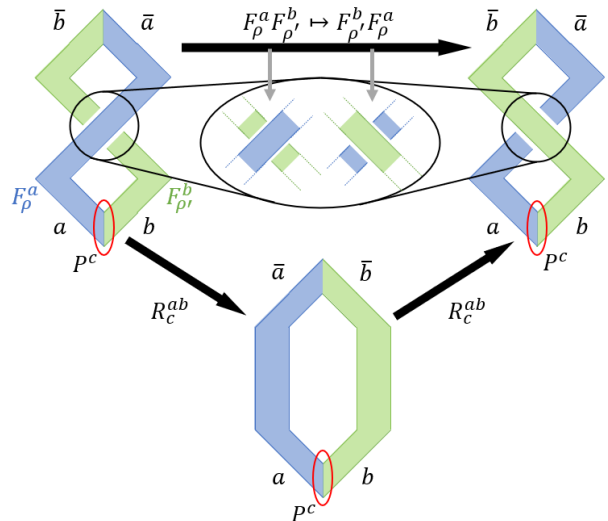


FIG. 4. Diagrammatic representation of anyonic braiding by manipulating ribbon operators F_{ρ}^a and $F_{\rho'}^b$, creating pairs of anyons (a, \bar{a}) and (b, \bar{b}) respectively to obtain the phase $(R_c^{ab})^2$. To highlight the topological equivalence of certain configurations, the ribbons ρ and ρ' are abstracted as smoothly deformable strips with no explicit construction on the lattice. In the top line we observe that exchange of order of operation of these two ribbons is equivalent to exchanging the paths on which they overlap. The bottom arrows show how to obtain the same configuration by two successive anyonic exchanges, each one characterised by R_c^{ab} , giving the relation $P^c F_{\rho}^a F_{\rho'}^b = (R_c^{ab})^2 P^c F_{\rho'}^b F_{\rho}^a$.

R_c^{ab} . A second clockwise braiding operation brings about another factor of R_c^{ab} giving eventually the final configuration on the right. In the anyonic basis such a set of transformations may be represented as

$$R_{\odot}^2 |a, b \rightarrow c\rangle = (R_c^{ab})^2 |a, b \rightarrow c\rangle, \quad (12)$$

where $R_{\odot} |a, b \rightarrow c\rangle$ describes the anti-clockwise exchange of anyons a and b with fixed fusion channel c .

By comparison of these two equivalent processes, we therefore observe that the values $(R_c^{ab})^2$ are encoded in the exchange of overlapping ribbon operators as

$$P^c F_{\rho}^a F_{\rho'}^b = (R_c^{ab})^2 P^c F_{\rho'}^b F_{\rho}^a. \quad (13)$$

In the following we show how to explicitly reconstruct the matrix $(R^{GG})^2$ with operations on the qudit lattice that encodes the $\mathbf{D}(S_3)$ quantum double model.

B. Deriving the R matrix on the $\mathbf{D}(S_3)$ lattice

Having demonstrated how the braiding of a pair of anyons may be implemented with ribbon operators we

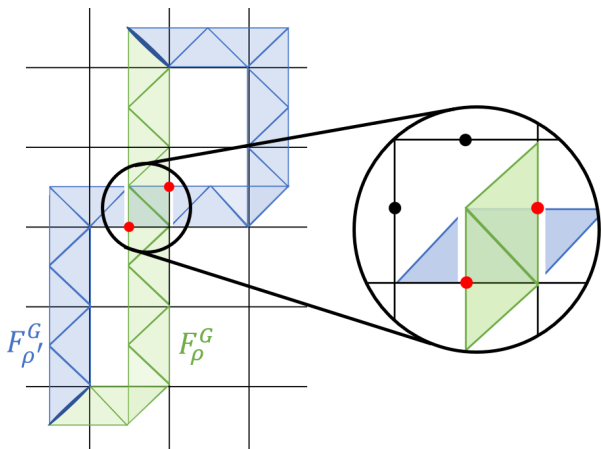


FIG. 5. Diagram illustrating the process to obtain the R^{GG} matrix on the quantum double lattice. Following Fig. 4 we illustrate a pair of braided G anyon ribbons, F_{ρ}^G and $F_{\rho'}^G$, with the same start and end points, highlighting the qudits where the ribbons cross. As the two ribbons, F_{ρ}^G and $F_{\rho'}^G$, cross at two qudits, denoted with red dots, the effect of the braiding only depends on the action on these qudits. Hence, the elements $(R_i^{GG})^2$ may be reproduced by the reduced system of two simple ribbons, $F_{\rho_1}^G$ and $F_{\rho_2}^G$, as shown in Fig. 6.

now want to show how the abstract diagrams of ribbons in Figure 4 may be explicitly realised on a lattice. Consider the ribbons F_{ρ}^G and $F_{\rho'}^G$ shown in Figure 5. In the previous section we have shown how topological invariance allows these ribbons to take any arbitrary homotopically equivalent shape as long as the structure of this overlap, which encodes their braiding information, is preserved. Hence, the commutativity of two arbitrary ribbons reduces down to the commutativity of the operators acting on these two points of overlap. These minimal operators are $F_{\rho_1}^G$ and $F_{\rho_2}^G$ described by (C20) and (C21) respectively and forming a crossed joint on the two qudits as shown in Figure 6. For this system, Equation (13) thus becomes

$$A^i(v)F_{\rho_2}^G F_{\rho_1}^G = (R_i^{GG})^2 A^i(v)F_{\rho_1}^G F_{\rho_2}^G \quad (14)$$

where $A^i(v)$, $i = A, B, G$, is the vertex projector as defined in (C22), projecting onto the desired fusion outcome of anyons G_1 and G_2 as in Figure 6.

In order to extract the braiding information from these operators we thus introduce two sets of states

$$\begin{aligned} |\phi_{21}(i)\rangle &= N_i A^i(v) F_{\rho_2}^G F_{\rho_1}^G |\zeta\rangle, \\ |\phi_{12}(j)\rangle &= N_j A^j(v) F_{\rho_1}^G F_{\rho_2}^G |\zeta\rangle, \end{aligned} \quad (15)$$

for $i, j = A, B, G$, with normalisation factors $N_A = N_B = 2$ and $N_G = \sqrt{2}$ required due to the action of the projectors such that $\langle \phi_{21}(i) | \phi_{21}(i') \rangle = \langle \phi_{12}(i) | \phi_{12}(i') \rangle = \delta_{ii'}$.

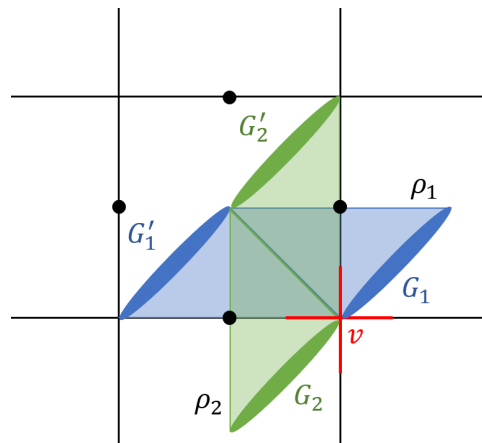


FIG. 6. The positions of the four G dyons are depicted as created by the operators $F_{\rho_1}^G F_{\rho_2}^G$ and $F_{\rho_2}^G F_{\rho_1}^G$. Anyons G'_1 and G'_2 overlap on a plaquette, while G_1 and G_2 overlap on the vertex labelled v . By applying a vertex projector $A^i(v)$, $i = A, B$ or G , the outcome of the fusion $G_1 \times G_2$ can be directly measured.

By analogy with Equation (14), we thus have

$$|\phi_{21}(i)\rangle = (R_i^{GG})^2 |\phi_{12}(i)\rangle \quad (16)$$

such that the algebraic form of each element $(R^{GG})_i^i \equiv R_i^{GG}$ corresponds to the result of the calculation of the overlap

$$(R_i^{GG})^2 = \langle \phi_{12}(i) | \phi_{21}(i) \rangle. \quad (17)$$

By explicit computation of these amplitudes we obtain

$$(R_A^{GG})^2 = (R_B^{GG})^2 = \bar{\omega}, \quad (R_G^{GG})^2 = \omega, \quad (18)$$

demonstrating the exact reconstruction of $(R^{GG})^2$ in the anyonic basis. Hence, by considering only the two segments ρ_1 and ρ_2 of the braiding ribbons ρ and ρ' we are able to determine the braiding matrix of the G anyons squared. In Appendix E we provide an alternative derivation of this result with the evaluation of the operator products $F_{\rho_1}^G F_{\rho_2}^G$ and $F_{\rho_2}^G F_{\rho_1}^G$ in the basis of group elements. With comparison of the elements of the resulting matrices, $(R^{GG})^2$ may be derived in the anyonic basis in a method lending itself to the quantum tomographic verification of [39].

IV. F MATRIX DERIVATION

We will now determine the fusion recombination matrix, F , illustrated in Figure 1(b). Together with the R matrix determined in the previous section, the evaluation of the F matrix will enable us to show their non-commutativity

and thus demonstrate the non-Abelian character of the G anyons of $\mathbf{D}(\mathbf{S}_3)$. Here we provide a minimal set of ribbon operators and local projections of the planar code model that can determine each of the matrix elements $(F_{GGG}^G)_j^i$.

Surprisingly, the evaluated quantum amplitudes provide the F matrix elements *squared*. This ‘doubling’ of fusion processes is obtained when considering the action of ribbon operators on a closed system of anyons, where total charge must be conserved. However, we will show that the obtained information is sufficient to explicitly verify that the matrices F_{GGG}^G and R^{GG} do not commute, and thus demonstrate the non-Abelianity of $\mathbf{D}(\mathbf{S}_3)$.

A. The doubling of fusion recombination

The matrix F_{GGG}^G describes the change of basis in the Hilbert space of four G anyons happening when we exchange the order of fusion of three distinct G anyons, G_1, G_2, G_3 to a fourth composite G_4 anyon. In the notation of Equation (4) we have

$$\begin{aligned} & |(G_1, G_2), G_3 \rightarrow i, G_3 \rightarrow G_4\rangle \\ &= \sum_j (F_{GGG}^G)_j^i |G_1, (G_2, G_3) \rightarrow G_1, j \rightarrow G_4\rangle. \end{aligned} \quad (19)$$

Equivalently, the orthogonality of distinct fusion channels means that each matrix element $(F_{GGG}^G)_j^i$ may be expressed as the overlap

$$\begin{aligned} & (F_{GGG}^G)_j^i = \\ & \langle G_1, (G_2, G_3) \rightarrow G_1, j \rightarrow G_4 | (G_1, G_2), G_3 \rightarrow i, G_3 \rightarrow G_4 \rangle. \end{aligned}$$

To successfully simulate this process on the lattice, we therefore want to develop a methodology that allows for the controlled re-ordering of the fusion of three G anyons and the intermediary composite i or j . Akin to the methodology for the R matrix, the fusion of G anyons is enacted with the application of combinations of ribbons producing pairs of these anyons $(G_n, G'_n), n = 1, 2, 3, 4$ as shown in Figure 7. The ordering of fusion is controlled by the application of projective measurements to a chosen pair of anyons. For example, in Fig. 7(a) the first measurement is of G_1 and G_2 to fusion outcome i , whereas in Fig. 7(b), the creation of j is ensured by the projection onto the fusion of G_2 and G_3 . We note that each of our states is constructed from the application of ribbon operators to the vacuum. Superselection therefore dictates that at each stage it must always be possible to fuse the created anyons back to the vacuum. As each of the ribbon operators in the quantum double necessarily create anyons in pairs, we will see that anyonic conservation therefore results in two identical fusion

processes occurring simultaneously between two sets of anyons, (G_1, G_2, G_3, G_4) and (G'_1, G'_2, G'_3, G'_4) as shown in Figure 7.

To make this analysis explicit, we denote the two sets of identical fusion processes with the tensor product such that in the anyonic basis we obtain

$$\begin{aligned} |\Psi_1(i)\rangle &= |(G_1, G_2), G_3 \rightarrow i, G_3 \rightarrow G\rangle \\ &\otimes |(G'_1, G'_2), G'_3 \rightarrow i, G'_3 \rightarrow G\rangle \end{aligned} \quad (20)$$

and

$$\begin{aligned} |\Psi_2(j)\rangle &= |G_1, (G_2, G_3) \rightarrow G_1, j \rightarrow G\rangle \\ &\otimes |G'_1, (G'_2, G'_3) \rightarrow G'_1, j \rightarrow G\rangle. \end{aligned} \quad (21)$$

It is important here to note that although the matrix F_{GGG}^G relates two sets of orthonormal basis states as in Equation (4), this doubling of fusion processes produced by projection operators is described by the non-unitary matrix with elements $\mathcal{F}_j^i = [(F_{GGG}^G)_j^i]^2$. In order to extract these elements it is therefore necessary to choose one set of states as an orthonormal basis. The set of states created by re-ordering the fusion processes as detailed may then not be orthonormal, but can be expressed as a linear combination of the other set of states. For example, if $|\Psi_2(j)\rangle$ is constructed as the orthonormal basis, then

$$|\Psi_1(i)\rangle = \sum_j [(F_{GGG}^G)_j^i]^2 |\Psi_2(j)\rangle \quad (22)$$

In this way we obtain

$$\langle \Psi_2(j) | \Psi_1(i) \rangle = [(F_{GGG}^G)_j^i]^2, \quad (23)$$

where one $(F_{GGG}^G)_j^i$ comes from the recombination of the unprimed G anyons and the other from the primed ones. Such a method for reproducing the F matrix using a closed system will therefore necessarily produce the squared value of each element. This is a general result differing from the case of the braiding procedure we saw in Section III B that produces $(R^{GG})^2$, which is due to the minimal size of the ribbons we consider. Below, we will introduce a set of states that explicitly demonstrate these anyonic processes with the quantum double lattice model.

B. Deriving the F matrix on the $\mathbf{D}(\mathbf{S}_3)$ lattice

Here we introduce a method to explicitly determine the elements

$$\mathcal{F}_j^i = [(F_{GGG}^G)_j^i]^2. \quad (24)$$

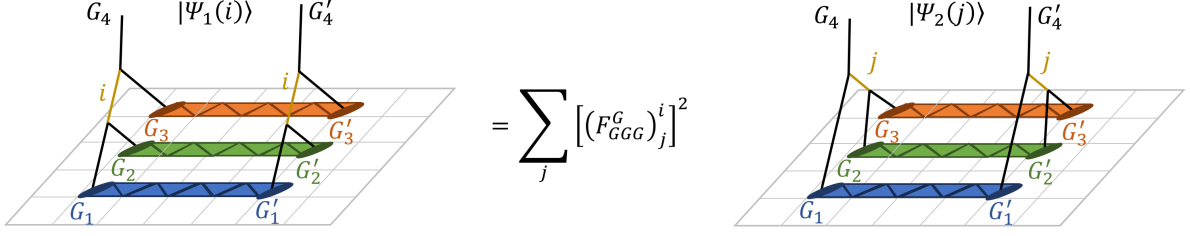


FIG. 7. Recombination in the fusion order of G anyons, as seen in Fig. 1(b), implemented on the $\mathbf{D}(\mathbf{S}_3)$ lattice. We consider three ribbons F_k^G , $k = 1, 2, 3$ that produce pairs of anyons G_k and G'_k at their endpoints. At one side of the ribbons we measure pairs of anyons in order to impose a certain fusion outcome. Each such measurement necessarily projects the anyons at the other endpoint to the same fusion outcome due to superselection rules. As a result, even if we manipulate only the anyons at one end of the ribbons, the process is doubled and the total state of the system produces squared amplitudes $[(F_{GGG}^G)_j^i]^2$ during fusion recombination, as seen in Equation (22).

of the ‘squared’ matrix \mathcal{F} , by considering operations on the lattice of the $\mathbf{D}(\mathbf{S}_3)$ quantum double model. Our main aim is to determine these matrix elements with the minimal amount of resources. In particular, we use the two qudit ribbons $F_{\rho_1}^G$ and $F_{\rho_2}^G$ defined in (C20) and (C21). As these ribbons overlap extra care must be taken to account for possible braiding phase factors, as we shall see in the following. We start by introducing two states

$$\begin{aligned} |\psi_1(i)\rangle &= A^{G_4}(v) F_{\rho_2}^{G_3} A^i(v) F_{\rho_2}^{G_2} F_{\rho_1}^{G_1} |\zeta\rangle, \\ |\psi_2(j)\rangle &= A^{G_4}(v) F_{\rho_1}^{G_3} A^j(v) F_{\rho_2}^{G_3} F_{\rho_2}^{G_2} |\zeta\rangle, \end{aligned} \quad (25)$$

for $i, j = A, B, G$. The subscripts in G_n are provided here to elucidate the link to the process shown in Figure 7, but will be dropped in the following when the distinction is not needed. Both states $|\psi_1(i)\rangle$ and $|\psi_2(j)\rangle$ are not normalised due to the application of the projectors $A^i(v)$. Nevertheless, states $|\psi_2(j)\rangle$ are orthogonal so in the following we account explicitly for their normalisation, $\langle \psi_2(j) | \psi_2(j) \rangle$. The states $|\psi_1(i)\rangle$ are not orthogonal to each other, but similar to (22) they can be represented as superpositions of $|\psi_2(j)\rangle$ states as

$$|\psi_1(i)\rangle = f_{iA} |\psi_2(A)\rangle + f_{iB} |\psi_2(B)\rangle + f_{iG} |\psi_2(G)\rangle. \quad (26)$$

As $|\psi_2(j)\rangle$ ’s are orthogonal we thus have

$$f_{ij} = \frac{\langle \psi_2(j) | \psi_1(i) \rangle}{\langle \psi_2(j) | \psi_2(j) \rangle}. \quad (27)$$

Similar to (23), the coefficients f_{ij} are related to the elements of the matrix \mathcal{F} up to overall phase factors generated due to the crossing of the ρ_1 and ρ_2 ribbons.

In the states $|\psi_1(i)\rangle$ and $|\psi_2(j)\rangle$, the order of fusion is explicitly enforced with the order of application of each of the ribbon operators, $F_{\rho_1}^G$ and $F_{\rho_2}^G$ to the ground state $|\zeta\rangle$. Consider $|\psi_1(i)\rangle$, the initial action of $F_{\rho_2}^G F_{\rho_1}^G$ on the anyonic vacuum $|\zeta\rangle$ produces two pairs of G anyons as

illustrated in Figure 6. By applying the projector $A^i(v)$ to the vertex v on which two of these anyons from different ribbons overlap, we may ensure the fusion outcome $G_1 \times G_2 \rightarrow i$. Superselection also ensures the simultaneous complementary fusion process $G'_1 \times G'_2 \rightarrow i$. The second application of $F_{\rho_2}^G$ to this state produces a subsequent pair of fusion processes in which the anyons G_3 and G'_3 fuse with the composite i anyons. The application of the final projector $A^G(v)$ to this vertex ensures that both $G_3 \times i \rightarrow G_4$ and $G'_3 \times i \rightarrow G'_4$, thus completing the construction of the fusion trees as shown in Figure 7. Note that as we require the use of a small system to realise the fusion properties, the ribbon operators used in $|\psi_1(i)\rangle$ and $|\psi_2(j)\rangle$ are crossing each other, giving rise to additional braiding phase factors.

With analytic consideration of the overlaps $\langle \psi_2(j) | \psi_1(i) \rangle$ as shown in Appendix F, we find that it is always possible to extract a phase factor $(R_G^{Gj})^2$ due to the braiding of the worldlines of the j and G_3 anyons in $|\psi_2(j)\rangle$. In particular, we have

$$\langle \psi_2(j) | \psi_1(i) \rangle = (R_G^{Gj})^2 \langle \zeta | F_{\rho_1}^G F_{\rho_2}^j A^G(v) F_{\rho_2}^G A^i(v) F_{\rho_2}^G F_{\rho_1}^G |\zeta\rangle. \quad (28)$$

We therefore find that, by using (25) and (26), the fusion matrix elements squared may be calculated from

$$\mathcal{F}_j^i = \overline{(R_G^{Gj})^2} f_{ij}, \quad (29)$$

where the phases

$$(R_G^{GA})^2 = (R_G^{GB})^2 = 1, \quad (R_G^{GG})^2 = \omega. \quad (30)$$

Calculation of these overlaps thus yields the ‘squared’ F matrix

$$\mathcal{F} = \frac{1}{4} \begin{pmatrix} 1 & 1 & 2 \\ 1 & 1 & 2 \\ 2 & 2 & 0 \end{pmatrix}. \quad (31)$$

This result is in agreement with the F -matrix of the G anyons of $\mathbf{D}(\mathbf{S}_3)$ given in (5), as determined from the pentagon equations. As this matrix is real and positive the values of the F matrix elements can be derived up to a sign ambiguity, due to the doubling of the fusion processes when ribbons are employed in the fusion recombination, as described in Fig. 7. In the following we show that the non-commutativity of the R^2 and F matrices can be demonstrated without the need to determine the value of these signs.

C. Non-Commutativity of F and R^2 matrices

In the previous we employed manipulations on the lattice of the $\mathbf{D}(\mathbf{S}_3)$ quantum double model to determine the elements of the fusion matrix, F . As the method we employed gives rise to squares of the elements, $\mathcal{F}_j^i = \left[(F_{GGG}^G)_j^i \right]^2$, a sign ambiguity arises in determining the elements of F_{GGG}^G when extracted from \mathcal{F} . It is possible however, to unequivocally show that for any valid combination of signs, we will always reproduce the desired non-commutativity, $[(R^{GG})^2, F_{GGG}^G] \neq 0$, which is the goal of this investigation.

To proceed we consider all matrices \tilde{F}_{GGG}^G that satisfy

$$\mathcal{F}_j^i = \left[\left(\tilde{F}_{GGG}^G \right)_j^i \right]^2. \quad (32)$$

We note that all such matrices must be unitary, and additionally due to the physical structure of the fusion process, must be real and symmetric. All such matrices may therefore be parameterised as

$$\left\{ \tilde{F}_{GGG}^G \right\} = \left\{ \frac{1}{2} \begin{pmatrix} \alpha & \beta & \gamma\sqrt{2} \\ \beta & \delta & \epsilon\sqrt{2} \\ \gamma\sqrt{2} & \epsilon\sqrt{2} & 0 \end{pmatrix}, \alpha, \beta, \gamma, \delta, \epsilon = \pm 1 \right\} \quad (33)$$

where the additional constraint of unitarity yields only eight possible solutions. For each such matrix the commutator between $(R^{GG})^2$ and \tilde{F}_{GGG}^G takes the form

$$\left[(R^{GG})^2, \tilde{F}_{GGG}^G \right] = \frac{1}{2} \begin{pmatrix} 0 & 0 & i\gamma\sqrt{6} \\ 0 & 0 & i\epsilon\sqrt{6} \\ -i\gamma\sqrt{6} & -i\epsilon\sqrt{6} & 0 \end{pmatrix} \neq \mathbf{0}, \quad (34)$$

for any value of $\gamma = \pm 1$ and $\epsilon = \pm 1$. Non-commutativity of $(R^{GG})^2$ and F_{GGG}^G also implies that R^{GG} and F_{GGG}^G do not commute. Hence, the simple lattice manipulations described above allow us to explicitly re-derive the non-commutativity of the G anyon exchange and fusion matrices, verifying their non-trivial braiding statistics as captured by the operator $(b_2)^2$ of equation (7).

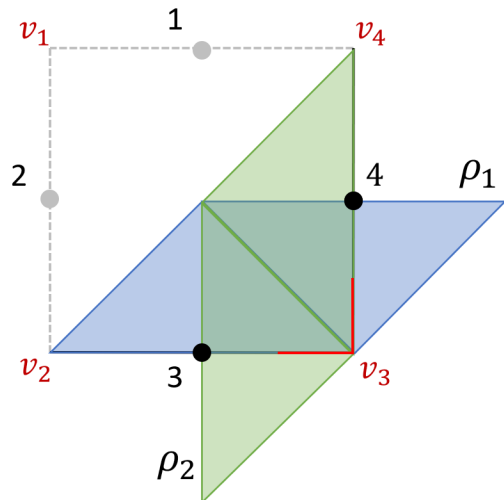


FIG. 8. The Kitaev Hamiltonian (9) defined on a single plaquette with open boundary conditions. In this system, both the ribbon operators $F_{\rho_1}^G$ and $F_{\rho_2}^G$ and projector $A^i(v_3)$ have support on only qudits 3 and 4, facilitating a dense encoding of the lattice reconstruction of the R and F matrices.

V. RECONSTRUCTING R AND F MATRICES WITH TWO $d = 6$ QUDITS

Our considerations thus far have been applicable to a quantum double lattice of arbitrary size. Here we will show that, by appropriate state preparation and manipulation, the whole process of determining $(R^{GG})^2$ and F_{GGG}^G described above can be encoded on two qudits only.

We start by considering the minimal lattice composed of four qudits on a single plaquette, p , with open boundary conditions as shown in Fig. 8. The Hamiltonian of the system is given by

$$\mathcal{H}_4 = -B(p) - \sum_{i=1}^4 A(v_i), \quad (35)$$

where the vertex operators, $A(v_i)$, act non-trivially on only two qudits. These reduced vertex projection operators act as boundary terms in the Hamiltonian (35). We note that the choice of boundary conditions for this minimal case is made without loss of generality but only to ensure that the corresponding model \mathcal{H}_4 has a unique ground state, $|\eta\rangle$, that has support on all four qudits. When creating pairs of G dyons with the application of $F_{\rho_1}^G$ and $F_{\rho_2}^G$ to $|\eta\rangle$, only a single flux is supported by this plaquette, the flux of the G dyon at the other end of the ribbon will lie outside of the system and thus cannot be directly measured.

In Equations (17) and (29) we have shown that the derivation of the forms of both the R and F matrices can

be expressed in terms of the overlap between the generalised states $|\phi_{12}(i)\rangle$ & $|\phi_{21}(j)\rangle$ and $|\psi_1(i)\rangle$ & $|\psi_2(j)\rangle$, respectively. For the case of a single plaquette system the states $|\phi_{12}(i)\rangle$ and $|\phi_{21}(j)\rangle$ are given by

$$\begin{aligned} |\phi_{12}(i)\rangle &= N_i A^i(v_3) F_{\rho_1}^G F_{\rho_2}^G |\eta\rangle, \\ |\phi_{21}(j)\rangle &= N_j A^j(v_3) F_{\rho_2}^G F_{\rho_1}^G |\eta\rangle, \end{aligned} \quad (36)$$

while $|\psi_1(i)\rangle$ and $|\psi_2(j)\rangle$ become

$$\begin{aligned} |\psi_1(i)\rangle &= A^G(v_3) F_{\rho_2}^G A^i(v_3) F_{\rho_2}^G F_{\rho_1}^G |\eta\rangle, \\ |\psi_2(j)\rangle &= A^G(v_3) F_{\rho_1}^G A^j(v_3) F_{\rho_2}^G F_{\rho_2}^G |\eta\rangle. \end{aligned} \quad (37)$$

The ribbon operators $F_{\rho_1}^G$ and $F_{\rho_2}^G$ act as defined in Equations (C20) and (C21) on qudits 3 and 4, as shown in Figure 8. Similarly, the projector $A^G(v_3)$ also acts on qudits 3 and 4, as seen in (G3). Hence, every operator in the amplitudes $\langle\phi_{21}(i)|\phi_{12}(i)\rangle$ and $\langle\psi_2(j)|\psi_1(i)\rangle$ only acts non-trivially on two qudits. It is possible to show (see Appendix G) that for any operator, O , that acts only on two qudits, its expectation value with respect to the four qudit ground state $|\eta\rangle$, can be given in terms of a two-qudit state by

$$\langle\eta|\mathbf{1}_{36} \otimes O|\eta\rangle = 6\langle\xi|O|\xi\rangle, \quad (38)$$

where

$$|\xi\rangle = \frac{1}{\sqrt{216}} \sum_{g_3, g_4 \in G} |g_3, g_4\rangle. \quad (39)$$

Here, $|\xi\rangle$, is a state that, similarly to O , has support on only the two qudits 3 and 4. Employing (38) and (39) one can directly determine $(R_i^{GG})^2 = \langle\phi_{21}(i)|\phi_{12}(i)\rangle$ and $[(F_{GG}^G)_j^i]^2 = (\overline{R_G^{Gj}})^2 \langle\psi_2(j)|\psi_1(i)\rangle$ by using only two $d = 6$ qudits, obtaining the same results as the full system. Hence, although the minimal physical system for implementing such an anyonic model is a single plaquette on four qudits, the ground state structure and reduced action of associated operators allows for the same information on the R and F matrix structure to be extracted from the overlaps of states constructed on two qudits.

VI. CONCLUSION

This work represents a significant step towards the realisation of non-Abelian anyons in practical quantum systems, offering a clear pathway for experimental demonstration and potential applications in quantum information processing and error correction. To achieve this, we have bridged the gap between the abstract manipulations that give rise to non-Abelian statistics and the specific steps required to conclusively demonstrate their non-Abelianity in a possible physical realisation. For this

task, we considered the $\mathbf{D}(\mathbf{S}_3)$ quantum double model, which supports the closed anyonic subgroup $\{A, B, G\}$, with G being the non-Abelian anyon. This model can be encoded on a square lattice of $d = 6$ qudits. While generating and manipulating G anyons in this model typically requires a lattice of several qudits and controlled operations between them, we have shown that by carefully investigating the braiding and fusion properties of the G anyons, this information can be decoded from the ribbons that generate them using simple projective measurements. Furthermore, we developed a scheme whereby the R and F matrices of the G anyons can be determined using only two qudits, significantly reducing the experimental resources required to demonstrate non-Abelian statistics.

Physical implementations of non-Abelian anyonic systems present significant experimental challenges due to the need for precise control over fusion and braiding operations. Various platforms, including superconducting circuits, trapped ions, and cold atoms, have been explored for simulating anyonic dynamics, each with distinct advantages and limitations. In particular, photonic systems have emerged as a powerful candidate for simulating non-Abelian anyons due to their inherent ability to implement high-fidelity projective measurements and non-unitary operations. As demonstrated in previous work [39], photonic platforms allow the encoding of anyonic degrees of freedom in high-dimensional spatial modes, where non-Abelian fusion and braiding matrices can be implemented with high precision using spatial light modulators and mode-mixing elements. This approach has been successfully used to realise a proof-of-concept simulation of the $\mathbf{D}(\mathbf{S}_3)$ anyonic model, achieving non-unitary transformations with fidelities above 94% [39]. Additionally, photonic setups are well-suited for simulating the effects of noise, decoherence, and error mitigation strategies in anyonic systems, complementing recent efforts in noisy quantum circuit simulations [25, 26]. In this work, we build on these advances to explore the minimal physical requirements for observing non-Abelian anyonic statistics, with a focus on qudit-based lattice implementations that are experimentally feasible with current photonic and cold-atom technologies. Our analysis highlights the key primitive operations—state preparation, braiding, fusion, and measurement—and their experimental realisability, providing a pathway toward near-term demonstrations of non-Abelian anyons.

ACKNOWLEDGMENTS

This work was supported by EPSRC with Grant No. EP/R020612/1. L.B. acknowledges support from EP-

-
- [1] J. Leinaas and J. Myrheim, “On the theory of identical particles,” *Il nuovo cimento*, vol. 37, p. 132, 1977.
- [2] A. Y. Kitaev, “Fault-tolerant quantum computation by anyons,” *Annals of physics*, vol. 303, no. 1, pp. 2–30, 2003.
- [3] C. Nayak, S. H. Simon, A. Stern, M. Freedman, and S. Das Sarma, “Non-abelian anyons and topological quantum computation,” *Reviews of Modern Physics*, vol. 80, no. 3, pp. 1083–1159, 2008.
- [4] J.-K. Li, K. Sun, Z.-Y. Hao, J.-H. Liang, S.-J. Tao, J. K. Pachos, J.-S. Xu, Y.-J. Han, C.-F. Li, and G.-C. Guo, “Photonic simulation of majorana-based jones polynomials,” *arXiv preprint arXiv:2403.04980*, 2024.
- [5] E. Dennis, A. Kitaev, A. Landahl, and J. Preskill, “Topological quantum memory,” *Journal of Mathematical Physics*, vol. 43, no. 9, pp. 4452–4505, 2002.
- [6] B. M. Terhal, “Quantum error correction for quantum memories,” *Reviews of Modern Physics*, vol. 87, no. 2, pp. 307–346, 2015.
- [7] S. Roberts and S. D. Bartlett, “Symmetry-protected self-correcting quantum memories,” *Physical Review X*, vol. 10, no. 3, p. 031041, 2020.
- [8] S. Bravyi and J. Haah, “Quantum self-correction in the 3d cubic code model,” *Physical review letters*, vol. 111, no. 20, p. 200501, 2013.
- [9] B. Yoshida, “Feasibility of self-correcting quantum memory and thermal stability of topological order,” *Annals of Physics*, vol. 326, no. 10, pp. 2566–2633, 2011.
- [10] X. Shen, Z. Wu, L. Li, Z. Qin, and H. Yao, “Fracton topological order at finite temperature,” *Physical Review Research*, vol. 4, no. 3, p. L032008, 2022.
- [11] C. Chamon, “Quantum glassiness in strongly correlated clean systems: An example of topological overprotection,” *Physical review letters*, vol. 94, no. 4, p. 040402, 2005.
- [12] R. Raussendorf, J. Harrington, and K. Goyal, “Topological fault-tolerance in cluster state quantum computation,” *New Journal of Physics*, vol. 9, no. 6, p. 199, 2007.
- [13] M. A. Nielsen, “Optical quantum computation using cluster states,” *Physical review letters*, vol. 93, no. 4, p. 040503, 2004.
- [14] G. Moore and N. Read, “Nonabelions in the fractional quantum hall effect,” *Nuclear Physics B*, vol. 360, no. 2-3, pp. 362–396, 1991.
- [15] S. Das Sarma, M. Freedman, and C. Nayak, “Topologically protected qubits from a possible non-abelian fractional quantum hall state,” *Physical review letters*, vol. 94, no. 16, p. 166802, 2005.
- [16] M. Dolev, M. Heiblum, V. Umansky, A. Stern, and D. Mahalu, “Observation of a quarter of an electron charge at the $\nu=5/2$ quantum hall state,” *Nature*, vol. 452, no. 7189, pp. 829–834, 2008.
- [17] N. Read and D. Green, “Paired states of fermions in two dimensions with breaking of parity and time-reversal symmetries and the fractional quantum hall effect,” *Physical Review B*, vol. 61, no. 15, p. 10267, 2000.
- [18] D. A. Ivanov, “Non-abelian statistics of half-quantum vortices in p-wave superconductors,” *Physical review letters*, vol. 86, no. 2, p. 268, 2001.
- [19] S. Xu, Z.-Z. Sun, K. Wang, L. Xiang, Z. Bao, Z. Zhu, F. Shen, Z. Song, P. Zhang, W. Ren, *et al.*, “Digital simulation of projective non-abelian anyons with 68 superconducting qubits,” *Chinese Physics Letters*, vol. 40, no. 6, p. 060301, 2023.
- [20] e. a. Andersen, Trond I, “Non-abelian braiding of graph vertices in a superconducting processor,” *Nature*, vol. 618, no. 7964, pp. 264–269, 2023.
- [21] V. Mourik, K. Zuo, S. M. Frolov, S. Plissard, E. P. Bakkers, and L. P. Kouwenhoven, “Signatures of majorana fermions in hybrid superconductor-semiconductor nanowire devices,” *Science*, vol. 336, no. 6084, pp. 1003–1007, 2012.
- [22] P. Yu, J. Chen, M. Gomanko, G. Badawy, E. Bakkers, K. Zuo, V. Mourik, and S. Frolov, “Non-majorana states yield nearly quantized conductance in superconductor-semiconductor nanowire devices,” *arXiv preprint arXiv:2004.08583*, 2020.
- [23] M. Aguado, G. Brennen, F. Verstraete, and J. I. Cirac, “Creation, manipulation, and detection of abelian and non-abelian anyons in optical lattices,” *Physical review letters*, vol. 101, no. 26, p. 260501, 2008.
- [24] J.-S. Xu, K. Sun, Y.-J. Han, C.-F. Li, J. K. Pachos, and G.-C. Guo, “Simulating the exchange of majorana zero modes with a photonic system,” *Nature communications*, vol. 7, no. 1, p. 13194, 2016.
- [25] Z.-H. Liu, K. Sun, J. K. Pachos, M. Yang, Y. Meng, Y.-W. Liao, Q. Li, J.-F. Wang, Z.-Y. Luo, Y.-F. He, *et al.*, “Topological contextuality and anyonic statistics of photonic-encoded parafermions,” *PRX Quantum*, vol. 2, no. 3, p. 030323, 2021.
- [26] J. R. Wootton, “Demonstrating non-abelian braiding of surface code defects in a five qubit experiment,” *Quantum Science and Technology*, vol. 2, no. 1, p. 015006, 2017.
- [27] J. P. Stenger, N. T. Bronn, D. J. Egger, and D. Pekker, “Simulating the dynamics of braiding of majorana zero modes using an ibm quantum computer,” *Physical Review Research*, vol. 3, no. 3, p. 033171, 2021.
- [28] M. Iqbal, N. Tantivasadakarn, R. Verresen, S. L. Campbell, J. M. Dreiling, C. Figgatt, J. P. Gaebler, J. Johansen, M. Mills, S. A. Moses, *et al.*, “Non-abelian topological order and anyons on a trapped-ion processor,” *Nature*, vol. 626, no. 7999, pp. 505–511, 2024.
- [29] P. Bonderson, M. Freedman, and C. Nayak, “Measurement-only topological quantum computa-

- tion,” *Physical review letters*, vol. 101, no. 1, p. 010501, 2008.
- [30] P. Bonderson, M. Freedman, and C. Nayak, “Measurement-only topological quantum computation via anyonic interferometry,” *Annals of Physics*, vol. 324, no. 4, pp. 787–826, 2009.
- [31] X.-W. Luo, Y.-J. Han, G.-C. Guo, X. Zhou, and Z.-W. Zhou, “Simulation of non-abelian anyons using ribbon operators connected to a common base site,” *Physical Review A*, vol. 84, no. 5, p. 052314, 2011.
- [32] G. Brennen, M. Aguado, and J. I. Cirac, “Simulations of quantum double models,” *New Journal of Physics*, vol. 11, no. 5, p. 053009, 2009.
- [33] S. Beigi, P. W. Shor, and D. Whalen, “The quantum double model with boundary: condensations and symmetries,” *Communications in mathematical physics*, vol. 306, pp. 663–694, 2011.
- [34] Z. K. Mineev, K. Najafi, S. Majumder, J. Wang, A. Stern, E.-A. Kim, C.-M. Jian, and G. Zhu, “Realizing string-net condensation: Fibonacci anyon braiding for universal gates and sampling chromatic polynomials,” 2024.
- [35] S. Xu, Z.-Z. Sun, K. Wang, H. Li, Z. Zhu, H. Dong, J. Deng, X. Zhang, J. Chen, Y. Wu, C. Zhang, F. Jin, X. Zhu, Y. Gao, A. Zhang, N. Wang, Y. Zou, Z. Tan, F. Shen, J. Zhong, Z. Bao, W. Li, W. Jiang, L.-W. Yu, Z. Song, P. Zhang, L. Xiang, Q. Guo, Z. Wang, C. Song, H. Wang, and D.-L. Deng, “Non-abelian braiding of fibonacci anyons with a superconducting processor,” *Nature Physics*, July 2024.
- [36] S. Bseiso, J. Pommerening, R. R. Allen, S. H. Simon, and L. Hormozi, “Minimal quantum circuits for simulating fibonacci anyons,” 2024.
- [37] C.-Y. Lu, W.-B. Gao, O. Gühne, X.-Q. Zhou, Z.-B. Chen, and J.-W. Pan, “Demonstrating anyonic fractional statistics with a six-qubit quantum simulator,” *Physical review letters*, vol. 102, no. 3, p. 030502, 2009.
- [38] J. Pachos, W. Wiczeorek, C. Schmid, N. Kiesel, R. Pohlner, and H. Weinfurter, “Revealing anyonic features in a toric code quantum simulation,” *New Journal of Physics*, vol. 11, no. 8, p. 083010, 2009.
- [39] S. Goel, M. Reynolds, M. Girling, W. McCutcheon, S. Leedumrongwatthanakun, V. Srivastav, D. Jennings, M. Malik, and J. K. Pachos, “Unveiling the non-abelian statistics of $d(s=3)$ anyons via photonic simulation,” *arXiv preprint arXiv:2304.05286*, 2023.
- [40] H. Weimer, M. Müller, I. Lesanovsky, P. Zoller, and H. P. Büchler, “A rydberg quantum simulator,” *Nature Physics*, vol. 6, no. 5, pp. 382–388, 2010.
- [41] A. Benhemou, T. Angkhanawin, C. S. Adams, D. E. Browne, and J. K. Pachos, “Universality of $z=3$ parafermions via edge-mode interaction and quantum simulation of topological space evolution with rydberg atoms,” *Physical Review Research*, vol. 5, no. 2, p. 023076, 2023.
- [42] A. Kómár and O. Landon-Cardinal, “Anyons are not energy eigenspaces of quantum double hamiltonians,” *Physical Review B*, vol. 96, no. 19, p. 195150, 2017.
- [43] J. K. Pachos, *Introduction to topological quantum computation*. Cambridge University Press, 2012.
- [44] S. H. Simon, *Topological quantum*. Oxford University Press, 2023.
- [45] K. Laubscher, D. Loss, and J. R. Wootton, “Universal quantum computation in the surface code using non-abelian islands,” *Physical Review A*, vol. 100, no. 1, p. 012338, 2019.
- [46] S. Bravyi and A. Kitaev, “Universal quantum computation with ideal clifford gates and noisy ancillas,” *Physical Review A—Atomic, Molecular, and Optical Physics*, vol. 71, no. 2, p. 022316, 2005.
- [47] I. Cong, M. Cheng, and Z. Wang, “Universal quantum computation with gapped boundaries,” *Physical Review Letters*, vol. 119, no. 17, p. 170504, 2017.
- [48] S. X. Cui, S.-M. Hong, and Z. Wang, “Universal quantum computation with weakly integral anyons,” *Quantum Information Processing*, vol. 14, pp. 2687–2727, 2015.
- [49] H. Bombin and M. Martin-Delgado, “Family of non-abelian kitaev models on a lattice: Topological condensation and confinement,” *Physical Review B*, vol. 78, no. 11, p. 115421, 2008.
- [50] S. Bravyi, M. B. Hastings, and S. Michalakis, “Topological quantum order: stability under local perturbations,” *Journal of mathematical physics*, vol. 51, no. 9, 2010.
- [51] S. Bravyi and M. B. Hastings, “A short proof of stability of topological order under local perturbations,” *Communications in mathematical physics*, vol. 307, pp. 609–627, 2011.
- [52] O. Landon-Cardinal and D. Poulin, “Local topological order inhibits thermal stability in 2d,” *Physical review letters*, vol. 110, no. 9, p. 090502, 2013.
- [53] R. Alicki, M. Fannes, and M. Horodecki, “A statistical mechanics view on kitaev’s proposal for quantum memories,” *Journal of Physics A: Mathematical and Theoretical*, vol. 40, no. 24, p. 6451, 2007.
- [54] R. Alicki, M. Fannes, and M. Horodecki, “On thermalization in kitaev’s 2d model,” *Journal of Physics A: Mathematical and Theoretical*, vol. 42, no. 6, p. 065303, 2009.
- [55] Z. Nussinov and G. Ortiz, “Autocorrelations and thermal fragility of anyonic loops in topologically quantum ordered systems,” *Physical Review B—Condensed Matter and Materials Physics*, vol. 77, no. 6, p. 064302, 2008.
- [56] S. Iblisdir, D. Pérez-García, M. Aguado, and J. Pachos, “Scaling law for topologically ordered systems at finite temperature,” *Physical Review B—Condensed Matter and Materials Physics*, vol. 79, no. 13, p. 134303, 2009.
- [57] A. Prem, J. Haah, and R. Nandkishore, “Glassy quantum dynamics in translation invariant fracton models,” *Physical Review B*, vol. 95, no. 15, p. 155133, 2017.
- [58] D. Bacon, “Stability of quantum concatenated-code hamiltonians,” *Physical Review A—Atomic, Molecular, and Optical Physics*, vol. 78, no. 4, p. 042324, 2008.
- [59] J. R. Wootton, V. Lahtinen, and J. K. Pachos, “Universal quantum computation with a non-abelian topological memory,” in *Theory of Quantum Computation, Communication, and Cryptography: 4th Workshop, TQC 2009*,

Waterloo, Canada, May 11-13, 2009, *Revised Selected Papers 4*, pp. 56–65, Springer, 2009.

- [60] D. S. Wang, A. G. Fowler, A. M. Stephens, and L. C. Hollenberg, “Threshold error rates for the toric and surface codes,” *arXiv preprint arXiv:0905.0531*, 2009.
- [61] A. Kay and R. Colbeck, “Quantum self-correcting stabilizer codes,” *arXiv preprint arXiv:0810.3557*, 2008.
- [62] J. R. Wootton, “Quantum memories and error correction,” *Journal of Modern Optics*, vol. 59, no. 20, pp. 1717–1738, 2012.
- [63] J. R. Wootton, J. Burri, S. Iblidir, and D. Loss, “Error correction for non-abelian topological quantum computation,” *Physical review X*, vol. 4, no. 1, p. 011051, 2014.
- [64] F. Wilczek, “Quantum mechanics of fractional-spin particles,” *Physical review letters*, vol. 49, no. 14, p. 957, 1982.
- [65] L. Fiedler and P. Naaijken, “Haag duality for kitaev’s quantum double model for abelian groups,” *Reviews in Mathematical Physics*, vol. 27, no. 09, p. 1550021, 2015.
- [66] P. Naaijken, “Kitaev’s quantum double model from a local quantum physics point of view,” in *Advances in algebraic quantum field theory*, pp. 365–395, Springer, 2015.
- [67] G. Duclos-Cianci and D. Poulin, “Fast decoders for topological quantum codes,” *Physical review letters*, vol. 104, no. 5, p. 050504, 2010.
- [68] J. R. Wootton and D. Loss, “High threshold error correction for the surface code,” *Physical review letters*, vol. 109, no. 16, p. 160503, 2012.
- [69] J. R. Wootton, “Topological phases and self-correcting memories in interacting anyon systems,” *Physical Review A—Atomic, Molecular, and Optical Physics*, vol. 88, no. 6, p. 062312, 2013.
- [70] C. Mochon, “Anyon computers with smaller groups,” *Physical Review A*, vol. 69, no. 3, p. 032306, 2004.

Appendix A: Quantum simulations vs actual physical realisations of anyons

A natural question is how useful anyonic quantum simulations are, especially when considering minimal system sizes. To address this question we will consider various aspects of topological systems. A first desirable characteristic in topological quantum computation is the dynamical stability obtained by activating a Hamiltonian. It is known that the generated energy gap of topological Hamiltonians keeps the ground state resilient to erroneous perturbations [50, 51], which was the central characteristic that motivated the application of anyons to quantum computation [2]. Nevertheless, current quantum technology platforms have managed to minimise such perturbations to unprecedented levels making such a benefit against coherent errors rather redundant. The source of errors that impedes the realisation of quantum computers are incoherent errors, such as the presence of a finite temperature [52–56]. Typical anyonic systems are

equally exposed to such errors as other quantum computation platforms, with fractons offering a promising direction for resolving this problem [9–11, 57]. Hence, the requirement of a Hamiltonian can be relaxed without diminishing the applicability of the anyonic simulations.

Beyond the Hamiltonian protection, topological states are equivalent to quantum error correcting codes (QECCs) with high error thresholds, minimal resource requirements and an intuitive syndrome measurement procedure that stems from the 2D geometry of the topological systems [5, 58]. In this dictionary, the logical space of the QECC is identified with the Hilbert space of the anyons. Hence, realisation and manipulations of anyonic states with quantum simulators is a step towards building efficient quantum error correction in the laboratory. Such QECCs offer the ability to correct a sufficiently low level of incoherent errors, although, unlike the Hamiltonian protection against coherent errors, they need active monitoring and correction [59–61].

Another issue faced with quantum simulations is that their quantum degrees of freedom that encode the topological states do not necessarily possess a two-dimensional configuration. It should be noted that the exact position e.g. of the links or vertices of the quantum double lattice, is not important for realising the desired anyonic properties. Topological invariance means the quantum properties of the system do not depend on a metric and hence geometric characteristics are not relevant. Nevertheless, we do not want to lose the locality of the anyons, which stems from the locality of the plaquette and vertex operators of the quantum double model [2]. Indeed, as anyons are quasiparticles, they are expected to be localised in a finite region of the system. To preserve locality of the quantum double model we need to keep the information of the order of the qudits, e.g. by enumerating them, and we need to know their connectivity. This consideration also reflects on the locality of the syndrome measurements when the states are interpreted as a QECC, which is a desirable characteristic [5, 62].

We strongly believe that quantum simulation of small anyonic systems can become the seed for several future developments. The minimal system proposed here includes all the elements necessary to create the ecosystem of anyons and offers a proof-of-principle demonstration of anyonic properties. These few-qudit manipulations can be directly extended to larger systems when more qudits are available. Such an effort will allow the extension of our scheme to larger distance QECC and thus enhances the fault-tolerance of the system [63]. Furthermore, implementing the anyonic protocols described here with larger systems benchmarks the available quantum

technology towards various applications. Indeed, quantum double models can be directly connected to the fundamental physics of anyons [64], lattice gauge theories [65, 66], quantum error correction [67–69] and quantum computation [43, 44] thus providing a wide spectrum of applications.

Appendix B: The Quantum Double Model $\mathbf{D}(\mathbf{G})$

Here we provide an overview of the quantum double construction as first introduced in [2]. We start by outlining how the group \mathbf{G} defines the algebraic structure of the quantum double $\mathbf{D}(\mathbf{G})$, dictating the anyons present and their associated fusion and braiding relations. We will then go on to present the Kitaev quantum double model construction, in which these anyons appear as point-like excitations on a lattice of spins.

1. Anyons in the Quantum Double Model

For some finite group \mathbf{G} , the mathematical structure of the associated anyonic model is described by the Drinfeld double of the group. The different types of anyons are in one-to-one correspondence with the irreducible representations (irreps) of this operator algebra, and may therefore be uniquely specified by $(\mathcal{C}_g, \Gamma_{R(\mathcal{N}_g)}^{\mathcal{N}_g})$ where \mathcal{C}_g is the conjugacy class denoting an anyons magnetic flux

$$\mathcal{C}_g = \{hgh^{-1} | h \in \mathbf{G}\}, \quad (\text{B1})$$

\mathcal{N}_g is the normalizer of a group measuring the anyon's electric charge

$$\mathcal{N}_g = \{gh = hg | h \in \mathbf{G}\}, \quad (\text{B2})$$

and $R(\mathcal{N}_g)$ represents a unitary irrep of an element of the normaliser. Anyons that possess trivial charge (flux) are labelled fluxons (chargeons) and those with both non-trivial charge and flux are labelled dyons. We note that having trivial flux means that chargeons correspond to the conjugacy class $\mathcal{C}_e = \{e\}$, hence their normaliser will always be the group itself, $\mathcal{N}_e = \mathbf{G}$.

For any anyon labelled $(\mathcal{C}_g, \Gamma_{R(\mathcal{N}_g)}^{\mathcal{N}_g})$ its quantum dimensionality is given by

$$d(\mathcal{C}_g, \Gamma_{R(\mathcal{N}_g)}^{\mathcal{N}_g}) = |\mathcal{C}_g| |\Gamma_{R(\mathcal{N}_g)}^{\mathcal{N}_g}|, \quad (\text{B3})$$

Abelian anyons necessarily have $d = 1$ while all anyons with $d > 1$ are non-Abelian. The total quantum dimension, \mathcal{D} , of the model can be found from the sum of the quantum dimensions over all anyon types

$$\mathcal{D}^2 = \sum_{\text{anyons } k} d_k^2, \quad (\text{B4})$$

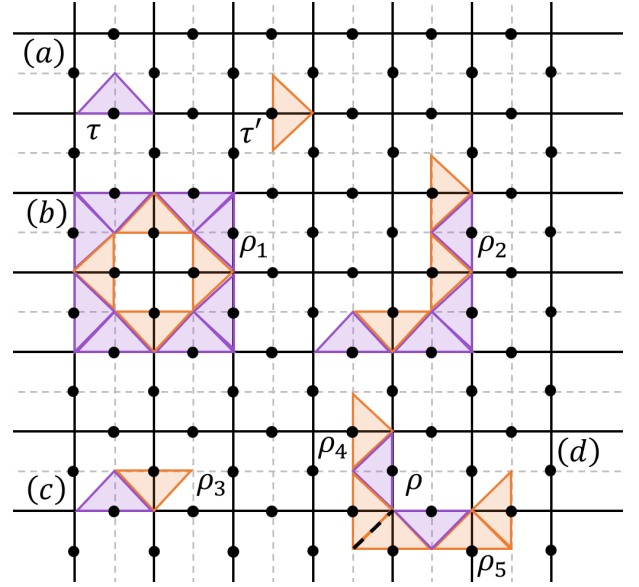


FIG. 9. The square lattice of the quantum double model with various triangle and ribbon operators. (a) The direct τ and dual τ' triangles formed from the L^g and T^h operators, respectively. (b) Closed loop, ρ_1 , and open-ended, ρ_2 , ribbon operators formed from combinations of triangle operators. (c) A ribbon operator with one dual and one direct triangle. (d) Two ribbons ρ_4 and ρ_5 that have been ‘glued’ together (shown by the dashed line on the connections of the triangles) to form a single extended ribbon ρ .

and is related to the cardinality of the chosen group

$$\mathcal{D}^2 = |\mathbf{G}|^2. \quad (\text{B5})$$

2. Ribbon Operators

Having outlined the abstract formalism for the classification of anyons in the quantum double model, we will now provide more detail on the ribbon operators with which they may be coherently created and transported on a two-dimensional lattice as shown in Figure 2.

For the quantum double $\mathbf{D}(\mathbf{G})$, an oriented lattice is constructed with a spin-like Hilbert space, \mathbf{H} , positioned on each link with orthonormal basis $\{|g\rangle : g \in \mathbf{G}\}$, such that $\dim(\mathbf{H}) = |\mathbf{G}|$. Four linear operators are introduced with action $L_+^g |z\rangle = |gz\rangle$, $L_-^g |z\rangle = |zg^{-1}\rangle$, $T_+^h |z\rangle = \delta_{h,z} |z\rangle$, $T_-^h |z\rangle = \delta_{h^{-1},z} |z\rangle$, for some $z, g, h \in \mathbf{G}$. The action of single-qudit operators L_\pm^g and T_\pm^h may be represented with dual and direct triangles respectively as shown in Fig. 9(a) (see Equations (C14) and (C15) for associated labelling convention). From these triangles, longer strips may be constructed as illustrated in Fig. 9(b). Any such strip is a valid ribbon as long as their direct and dual paths do not self-cross [49]. For

each ribbon ρ we introduce a set of operators $\{F_\rho^{h,g}\}$ with $h, g \in \mathbf{G}$, called ribbon operators. These operators act on all qudits contained in ρ , however their action is only non-trivial on the start and end sites (i.e. the ribbon operators commute with $A(v)$ and $B^e(p)$ for all sites other than the end sites). In this way, stabiliser violations corresponding to excitations of the system only arise at the endpoints of the ribbon.

In the simplest case, a ribbon may be constructed from a single triangle. If τ is a dual triangle and τ' a direct triangle, we set

$$F_\tau^{h,g} := \delta_{1,g} L_\tau^h, \quad F_{\tau'}^{h,g} := T_{\tau'}^g. \quad (\text{B6})$$

These ribbons have minimal length $l = 1$.

A ribbon is described as ‘proper’ if it is composed of at least one dual and one direct triangle. The smallest proper ribbon is thus composed of exactly one direct and one dual triangle as shown in Fig. 9(c). The associated ribbon operator is defined as the product of the ribbon operators on each triangle,

$$F_\rho^{h,g} = L_{\tau_{\text{dual}}}^h T_{\tau_{\text{dir}}}^g \quad (\text{B7})$$

For all general ribbons with $l > 1$, we may let $\rho = \rho_1 \rho_2$ and recursively define a ‘gluing’ procedure with the following

$$F_\rho^{h,g} := \sum_{k \in \mathbf{G}} F_{\rho_1}^{h,k} F_{\rho_2}^{\bar{k}h, \bar{k}g} \quad (\text{B8})$$

where the first site of ρ_2 is always the same as the last site of ρ_1 (see Fig. 9(d)).

These operators, $F_\rho^{h,g}$, allow for the construction of ribbon operators that give rise to X anyons at the endpoints of the path ρ . The construction of these is non-trivial as, unlike with the toric code [2], excitations in the form of spin rotations do not necessarily correspond to the creation of anyons [42].

For any Abelian anyon, ribbon operators giving rise to X anyons at the endpoints of the path ρ are given by [65]

$$F_\rho^{\chi,c} = \sum_{g \in S_3} \chi(g) F_\rho^{\bar{c},g} \quad (\text{B9})$$

where c is an element of \mathbf{G} and χ is a character representation of \mathbf{G} .

For non-Abelian anyons we must introduce the non-Abelian basis transformation [49]

$$F^{RC;\mathbf{u}\mathbf{v}} := \frac{n_R}{|\mathcal{N}_C|} \sum_{n \in \mathcal{N}_C} \bar{\Gamma}_R^{j,j'}(n) F^{\bar{c}_i, q_i n q_i'} \quad (\text{B10})$$

with each anyon having a unique conjugacy class \mathcal{C} and R , the irrep of the normaliser corresponding to \mathcal{C} , \mathcal{N}_C . The unitary matrices of the irrep are given as $\Gamma_R(g)$, $g \in \mathbf{G}$ and the dimension of this is given by n_R . Each element of the normaliser and conjugacy class are given by n_i and c_i respectively. The representation Q_C is defined by \mathbf{G}/\mathcal{N}_C and each element is given by q_i . Finally, $\mathbf{u} = (i, j)$ and $\mathbf{v} = (i', j')$ are additional degrees of freedom that may be traced out to give the final anyonic ribbon operator [45]. Examples of this construction for the Abelian A, B and non-Abelian G anyons of our chosen model are given in Appendix C.

Appendix C: Full Anyon Model $\mathbf{D}(\mathbf{S}_3)$

The anyons of the Drinfeld double of \mathbf{S}_3 are labeled by the conjugacy classes of \mathbf{S}_3 and the irreducible representations of the normalizers of these conjugacy classes. There are three conjugacy classes of S_3 :

$$\begin{aligned} \{\mathcal{C}_e\} &= \{e\}, \\ \{\mathcal{C}_c\} &= \{c, c^2\}, \\ \{\mathcal{C}_t\} &= \{t, tc, tc^2\}, \end{aligned} \quad (\text{C1})$$

with corresponding normalizers,

$$\begin{aligned} \mathcal{N}_e &= S_3, \\ \mathcal{N}_c &= \mathcal{N}_{c^2} = \{e, c, c^2\} \cong \mathbb{Z}_3, \\ \mathcal{N}_t &= \{e, t\} \cong \mathcal{N}_{tc} \cong \mathcal{N}_{tc^2} \cong \mathbb{Z}_2 \end{aligned} \quad (\text{C2})$$

where ‘ \cong ’ denotes an isomorphism [42]. The $\mathbf{D}(\mathbf{S}_3)$ quantum double model therefore consists of eight types of anyons labelled $\{A, B, C, D, E, F, G, H\}$, where each type of anyon corresponds to one of the eight irreducible representations of $\mathbf{D}(\mathbf{S}_3)$ as detailed in Table I. A denotes the vacuum particle with both trivial flux and charge, such that $A \times Z = Z$ for $Z \in \{A, B, \dots, H\}$.

Anyon	\mathcal{C}_g	\mathcal{N}_g	Irrep.	Q-dim.	Type
A	\mathcal{C}_e	S_3	$\Gamma_1^{S_3}$	1	Vacuum
B	\mathcal{C}_e	S_3	$\Gamma_{-1}^{S_3}$	1	Chargeon
C	\mathcal{C}_e	S_3	$\Gamma_2^{S_3}$	2	Chargeon
D	\mathcal{C}_t	\mathbb{Z}_2	$\Gamma_1^{\mathbb{Z}_2}$	3	Fluxon
E	\mathcal{C}_t	\mathbb{Z}_2	$\Gamma_{-1}^{\mathbb{Z}_2}$	3	Dyon
F	\mathcal{C}_c	\mathbb{Z}_3	$\Gamma_1^{\mathbb{Z}_3}$	2	Fluxon
G	\mathcal{C}_c	\mathbb{Z}_3	$\Gamma_\omega^{\mathbb{Z}_3}$	2	Dyon
H	\mathcal{C}_c	\mathbb{Z}_3	$\Gamma_{\bar{\omega}}^{\mathbb{Z}_3}$	2	Dyon

TABLE I. Anyons of $\mathbf{D}(\mathbf{S}_3)$ with their charge and flux labels, quantum dimensions and type.

In this work, we restrict to the non-Abelian sub-group $\{A, B, G\}$ which is closed under fusion as seen in

Equation (1). The irreps and character representations used in the construction of the ribbon operator creating pairs of these anyons as in (B9) and (B10) are detailed in Table II [39].

Anyon	Irrep.	e	c	c^2	t	tc	tc^2
A	$\Gamma_1^{\mathbf{S}_3}$	1	1	1	1	1	1
B	$\Gamma_{-1}^{\mathbf{S}_3}$	1	1	1	-1	-1	-1
G	$\Gamma_2^{\mathbf{S}_3}$	1	ω	$\bar{\omega}$	0	0	0

TABLE II. The irreducible representations of the submodel $\{A, B, G\}$ and the traces of their corresponding character irreducible representations.

Both Abelian anyons in our sub-model, $A : (\mathcal{C}_e = \{e\}, \Gamma_1^{\mathbf{S}_3})$ and $B : (\mathcal{C}_e = \{e\}, \Gamma_{-1}^{\mathbf{S}_3})$ in the $\mathbf{D}(\mathbf{S}_3)$ quantum double model correspond to the trivial conjugacy class \mathcal{C}_e and are therefore chargeons residing on the vertices of the lattice. The simplest ribbon capable of producing a pair of such anyons is a single-qudit direct triangle $\rho = \tau$ as shown in Figure 2(a). The forms of Eq.(C18) and (C19) arise from the substitution of this information into Equation (B9) with the character representations of Table II. For example, for a pair of B anyons

$$F_\tau^B \equiv F_\tau^{\chi(\Gamma_{-1}^{\mathbf{S}_3}), e}, \quad (\text{C3})$$

$$= F_\tau^{e,e} + F_\tau^{e,c} + F_\tau^{e,c^2} - F_\tau^{e,t} - F_\tau^{e,tc} - F_\tau^{e,tc^2}, \quad (\text{C4})$$

$$= T_+^e + T_+^c + T_+^{c^2} - T_+^t - T_+^{tc} - T_+^{tc^2}, \quad (\text{C5})$$

where we have applied the identity $F_\tau^{g,h} := T_\tau^h$ for a direct triangle τ seen in Equation (B6) and without loss of generality assumed that the triangle is facing along the oriented edge.

Similarly, for the non-Abelian anyons $G : (\mathcal{C}_c, \Gamma_\omega^{\mathbf{Z}_3})$ with irreducible representation as given in Table II, Equation (B10) yields

$$F_\rho^G = F_\rho^{c,e} + \omega F_\rho^{c,c} + \bar{\omega} F_\rho^{c,c^2} + F_\rho^{c^2,e} + \bar{\omega} F_\rho^{c^2,c} + \omega F_\rho^{c^2,c^2}. \quad (\text{C6})$$

The G anyon is dyonic, such that any ribbon ρ along which this operator may be applied, must be composed of at least one dual and one direct triangle. For ribbons ρ_1 and ρ_2 of the form $\rho = \tau_{\text{direct}}\tau_{\text{dual}}$, Equation (B7) is used to find the specific ribbon operators $F_{\rho_1}^G$ and $F_{\rho_2}^G$ given in Equations (C20) and (C21) respectively.

1. R and F Matrices

As briefly introduced in Section II, the sub-model $\{A, B, G\}$ has a non-trivial fusion as given in the fusion rules set out in (1), where the fusion multiplicity

of the G anyon signals its non-Abelian nature and subsequent potential for performing the non-trivial braiding key to the implementation of topological quantum computing schemes. Two G anyons have a three-dimensional Hilbert space indexed by each of the three orthogonal fusion channels as given in equation (1). In demonstrating the non-triviality of the braiding of these anyons it is constructive to begin by introducing the F and R matrices, the basic operations for the manipulation of anyons. The goal of this paper is to present a method in which these matrices can be reproduced with local operations on a lattice, thus explicitly demonstrating the non-Abelianity of the G anyons in the $\mathbf{D}(\mathbf{S}_3)$ quantum double model.

When two anyons labelled a and b undergo a counter-clockwise exchange, fusion commutativity $a \times b = b \times a$ dictates that their total charge c remains unchanged. Assigning a distinct basis state to each configuration, the swapping of two particles on a line therefore induces an isomorphism between these states described by the braiding operator

$$R_\circlearrowleft |a, b \rightarrow c\rangle = R_c^{ab} |a, b \rightarrow c\rangle \quad (\text{C7})$$

where R_\circlearrowleft corresponds to the anti-clockwise exchange of a and b anyons, as shown in Figure 1(a). For fusion processes with a unique fusion channel this mapping corresponds to the possible acquisition of a simple phase factor, R_c^{ab} . For the non-Abelian fusion of two G anyons, the fusion multiplicity generates a 3×3 diagonal unitary matrix R^{GG} with entries $(R^{GG})_i^i \equiv R_i^{GG}$, the form of which may be analytically determined using a set of self-consistent relations known as the pentagon and hexagon relations [43]. The matrix R^{GG} is found to take the form

$$R^{GG} = \begin{pmatrix} \omega & 0 & 0 \\ 0 & -\omega & 0 \\ 0 & 0 & \bar{\omega} \end{pmatrix}, \quad (\text{C8})$$

with $\omega = e^{\frac{2\pi i}{3}}$ and $\bar{\omega} = \omega^*$.

When considering the fusion of three anyons a, b, c to some fixed outcome d , the associated Hilbert space may be indexed by the possible intermediate fusion outcomes $a \times b \rightarrow i$ such that $i \times c \rightarrow d$ as shown on the left-hand side of Figure 1(b). Each state in this Hilbert space compactly takes the form $|(a, b), c \rightarrow i, c \rightarrow d\rangle$. Fusion associativity $(a \times b) \times c = a \times (b \times c)$ dictates that this same Hilbert space can equivalently be spanned by the states as represented on the right-hand side of Figure 1(b), for intermediary composite anyons j . Mapping between these two representations therefore requires the description of a basis transformation known as the fusion matrix F_{abc}^d . The action of this mapping may be

described in the anyonic basis as

$$|(a, b), c \rightarrow i, c \rightarrow d\rangle = \sum_j (F_{abc}^d)_j^i |a, (b, c) \rightarrow a, j \rightarrow d\rangle. \quad (\text{C9})$$

The fusion and braiding matrices R^{GG} and F_{GGG}^G display a non-commutativity

$$[R^{GG}, F_{GGG}^G] \neq 0, \quad (\text{C10})$$

thus making this sub-group $\{A, B, G\}$ a promising candidate for topological quantum computation. Moreover, this non-commutativity of the F and R matrices guarantees that our sub-model supports a non-trivial braiding matrix $b_2^G = (F_{GGG}^G)^{-1} R^{GG} F_{GGG}^G$, describing the braiding evolution between anyons that belong to different pairs. Clearly if F and R commute then $(b_2^G)^2 = (F_{GGG}^G)^{-1} (R^{GG})^2 F_{GGG}^G = (R^{GG})^2$ and thus all braiding operations commute with each other. In contrast the $\{A, B, C\}$ subgroup [59] with non-Abelian anyon C , has $(b_2^C)^2 = \mathbf{1}$ and thus does not offer non-commutative braiding operations [42, 63]. We note that while the fusion and braiding of G anyons alone is not sufficient for universal computation, such universality may be achieved with the addition of measurements to the protocol [48, 70]. The study of the fusion and braiding properties of these non-Abelian anyons is therefore still highly important to the potential realisation of fault-tolerant quantum computational schemes.

In a recent work [39] it was demonstrated how the matrix $(R^{GG})^2$ can be reproduced with the application of a pair of single qutrit G ribbons on a lattice. This minimal approach on a single qutrit could be efficiently simulated and verified using a quantum process tomography, thus providing the first step towards experimentally verifying the non-Abelianity of the G anyons in $\mathbf{D}(\mathbf{S}_3)$. Here, we build on this approach to introduce an alternative set of minimal operators with which we not only re-derive $(R^{GG})^2$, but also explicitly enact the swapping of the fusion order necessary to determine F_{GGG}^G . In this way we provide the first explicit verification of the non-commutativity of $(R^{GG})^2$ and F_{GGG}^G . Below we introduce the necessary components to realise the quantum double $\mathbf{D}(\mathbf{S}_3)$ on a lattice.

2. Lattice representation of the $\mathbf{D}(\mathbf{S}_3)$ model

We now present the lattice model that gives rise to the quantum double $\mathbf{D}(\mathbf{S}_3)$ presented above. This model, is based on the group structure of \mathbf{S}_3 , which is isomorphic to the symmetry transformations of an equilateral triangle, given by

$$\mathbf{S}_3 = \{e, c, c^2, t, tc, tc^2\}, \quad (\text{C11})$$

where c is the generator for rotations following $c^3 = e$, and t is the generator for reflections following $t^2 = e$ with e as the identity element. The non-Abelian nature of this group is defined by the relation $ct = tc^2$. Consider now a two-dimensional square lattice with orientation as shown in Figure 2. On each link of the lattice a Hilbert space described by $d = 6$ qudits is placed with orthonormal basis indexed by the group elements of \mathbf{S}_3 .

Four linear operators are introduced with action $L_+^g |z\rangle = |gz\rangle$, $L_-^g |z\rangle = |zg^{-1}\rangle$, $T_+^h |z\rangle = \delta_{h,z} |z\rangle$, $T_-^h |z\rangle = \delta_{h^{-1},z} |z\rangle$, for some $z, g, h \in \mathbf{S}_3$, on any six-dimensional qudit. These operators are represented by dual and direct triangles respectively, as shown in Figure 2(a). From these single-qudit operators a set of mutually commuting vertex

$$\begin{aligned} A(v) &= \frac{1}{6} \sum_{g \in \mathbf{S}_3} A^g(v), \\ &= \frac{1}{6} \sum_{g \in \mathbf{G}} L_{\pm}^g \otimes L_{\pm}^g \otimes L_{\pm}^g \otimes L_{\pm}^g, \end{aligned} \quad (\text{C12})$$

and plaquette operators

$$B^h(p) = \sum_{h_1 h_2 h_3 h_4 = h} T_{\pm}^{h_1} \otimes T_{\pm}^{h_2} \otimes T_{\pm}^{h_3} \otimes T_{\pm}^{h_4}, \quad (\text{C13})$$

may be constructed from closed loops of triangles as shown in Fig. 2(b). The choice of L_{\pm}^g and T_{\pm}^h in each operator are chosen in accordance with the following orientation convention

$$L_{\pm}^g = \begin{cases} L_+^g & \text{if edge is oriented into vertex,} \\ L_-^g & \text{if edge is oriented out of vertex,} \end{cases} \quad (\text{C14})$$

$$T_{\pm}^h = \begin{cases} T_+^h & \text{if edge is clockwise} \\ & \text{w.r.t. the plaquette,} \\ T_-^h & \text{if edge is anti-clockwise} \\ & \text{w.r.t. the plaquette.} \end{cases} \quad (\text{C15})$$

such that the vertex and plaquette operators as shown in Fig. 2(b) correspond to $A^g(v) = L_+^g \otimes L_-^g \otimes L_-^g \otimes L_+^g$ and $B^h(p) = \sum T_-^{h_1} \otimes T_-^{h_2} \otimes T_+^{h_3} \otimes T_+^{h_4}$ respectively. Assigning such an orientation convention to the single qudit operators ensures that all operators $A(v)$ and $B(p) \equiv B^e(p)$ are mutually commuting as discussed in Appendix D.

The Kitaev Hamiltonian [2]

$$\mathcal{H} = - \sum_v A(v) - \sum_p B(p), \quad (\text{C16})$$

defined on a lattice with open boundaries, produces a unique ground state $|\zeta\rangle$, corresponding to the anyonic vacuum, in which

$$A(v) |\zeta\rangle = |\zeta\rangle, \quad B(p) |\zeta\rangle = |\zeta\rangle, \quad (\text{C17})$$

for all vertices, v , and plaquettes, p . Particle-like excitations of this model are indicated by violations of the conditions (10).

The A and B anyons are both Abelian with trivial flux, and can therefore be created and moved with string operators corresponding to paths on the direct lattice as seen in Appendix B 2. In the simplest case, pairs of these anyons can be created on neighbouring vertices with the single-qudit operators

$$\begin{aligned} F_\tau^A &= T_+^e + T_+^c + T_+^{c^2} + T_+^t + T_+^{tc} + T_+^{tc^2} \\ &= |e\rangle \langle e| + |c\rangle \langle c| + |c^2\rangle \langle c^2| \\ &\quad + |t\rangle \langle t| + |tc\rangle \langle tc| + |tc^2\rangle \langle tc^2| \\ &\equiv \mathbf{1}_6 \end{aligned} \quad (\text{C18})$$

$$\begin{aligned} F_\tau^B &= T_+^e + T_+^c + T_+^{c^2} - T_+^t - T_+^{tc} - T_+^{tc^2} \\ &= |e\rangle \langle e| + |c\rangle \langle c| + |c^2\rangle \langle c^2| \\ &\quad - |t\rangle \langle t| - |tc\rangle \langle tc| - |tc^2\rangle \langle tc^2| \end{aligned} \quad (\text{C19})$$

represented as the direct triangles shown in Figure 2(a).

The G anyons are dyons that have both non-trivial flux and charge. They therefore require the implementation of ribbon operators composed of dual and direct triangles for their manipulation. In the following we will consider two distinct two-qudit ribbon operators

$$F_{\rho_1}^G = (T_-^e + \omega T_-^c + \bar{\omega} T_-^{c^2}) \otimes L_-^c + (T_-^e + \bar{\omega} T_-^c + \omega T_-^{c^2}) \otimes L_-^{c^2} \quad (\text{C20})$$

and

$$F_{\rho_2}^G = L_+^c \otimes (T_-^e + \omega T_-^c + \bar{\omega} T_-^{c^2}) + L_+^{c^2} \otimes (T_-^e + \bar{\omega} T_-^c + \omega T_-^{c^2}) \quad (\text{C21})$$

each composed of one direct and one dual triangle, as illustrated in Figure 2(c).

Finally, we will introduce a set of local measurement operators that may measure a specific anyon type laying on the selected vertex, with which the outcome A, B, G can be measured by

$$\begin{aligned} A^A(v) &= \frac{1}{6} \left(A^e(v) + A^c(v) + A^{c^2}(v) + A^t(v) \right. \\ &\quad \left. + A^{tc}(v) + A^{tc^2}(v) \right), \\ A^B(v) &= \frac{1}{6} \left(A^e(v) + A^c(v) + A^{c^2}(v) - A^t(v) \right. \\ &\quad \left. - A^{tc}(v) - A^{tc^2}(v) \right), \\ A^G(v) &= \frac{1}{3} \left(2A^e(v) - A^c(v) - A^{c^2}(v) \right), \end{aligned} \quad (\text{C22})$$

as in [42], which project onto the chosen anyon by measuring the charge. As each anyon in the $\{A, B, G\}$ sub-model has a unique charge, these vertex projectors are

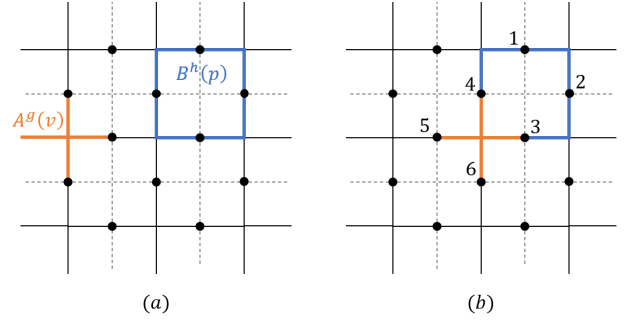


FIG. 10. (a) A four plaquette lattice with a vertex operator $A^g(v)$ and plaquette operator $B^h(p)$ acting on different qudits. (b) The same plaquette but with vertex and plaquette operators overlapping on two qudits 3 and 4.

sufficient in distinguishing between the possible anyons whose charge lies on a vertex v . Moreover, as the $\{A, B, G\}$ subgroup of anyons is closed there is no need to measure other type of anyons beyond these. Naturally, for the ground state anyonic vacuum, $|\zeta\rangle$, $A^A(v)|\zeta\rangle = |\zeta\rangle$ and $A^B(v)|\zeta\rangle = A^G(v)|\zeta\rangle = 0$, $\forall v$.

Appendix D: Commutativity of Vertex and Plaquette Operators

First, consider a plaquette operator $B^e(p)$ and a vertex operator $A(v)$. In calculating the commutation relation between any two such operators, there are two distinct cases as shown in Figure 10. In the first case, when both $A(v)$ and $B^e(p)$ act on two different sets of four qudits as in Fig.10(a), it is clear that they will necessarily commute. In the alternative non-trivial case where $A(v)$ and $B^e(p)$ ‘overlap’ and have non-trivial action on two of the same qudits on the lattice more care must be taken to demonstrate that these operators will commute.

Consider, for example, the operators $A(v)$ and $B^e(p)$ acting on the six qudits shown in Figure 10. For the labeling as shown these operators have the following forms

$$\begin{aligned} A(v) &= \frac{1}{6} \sum_{g \in \mathbf{G}} \mathbf{1} \otimes \mathbf{1} \otimes L_+^g \otimes L_+^g \otimes L_-^g \otimes L_-^g, \\ B^e(p) &= \sum_{h_1 h_2 h_3 h_4 = e} T_+^{h_1} \otimes T_-^{h_2} \otimes T_-^{h_3} \otimes T_+^{h_4} \otimes \mathbf{1} \otimes \mathbf{1}. \end{aligned} \quad (\text{D1})$$

The action on all unlabelled qudits on this lattice is trivial and can thus be ignored.

In order to show that $[A(v), B^e(p)] \equiv A(v)B^e(p) - B^e(p)A(v) = 0$ we expand out the form of each of the

products,

$$A(v)B^e(p) = \frac{1}{6} \sum_{g \in \mathbf{G}} \sum_{h_1 h_2 h_3 h_4 = e} T_+^{h_1} \otimes T_-^{h_2} \otimes L_+^g T_-^{h_3} \otimes L_+^g T_+^{h_4} \otimes L_-^g \otimes L_-^g \quad (\text{D2})$$

and

$$B^e(p)A(v) = \frac{1}{6} \sum_{g \in \mathbf{G}} \sum_{h_1 h_2 h_3 h_4 = e} T_+^{h_1} \otimes T_-^{h_2} \otimes T_-^{h_3} L_+^g \otimes T_+^{h_4} L_+^g \otimes L_-^g \otimes L_-^g. \quad (\text{D3})$$

In order to show that these two operators commute we refer to the commutation relations between the foundational L_\pm^g and T_\pm^h operators

$$L_+^g T_+^h = T_+^{hg} L_+^g, \quad L_-^g T_+^h = T_+^{hg^{-1}} L_-^g, \quad (\text{D4})$$

$$L_+^g T_-^h = T_+^{hg^{-1}} L_+^g, \quad L_-^g T_-^h = T_-^{hg} L_-^g, \quad (\text{D5})$$

as can be reproduced from the definitions of the action of L_\pm^g and T_\pm^h in Section C 2. The commutation identities in (D4) and (D5) yield $L_+^g T_-^{h_3} = T_+^{h_3 g^{-1}} L_+^g$ and $L_+^g T_+^{h_4} = T_+^{g h_4} L_+^g$ such that (D2) becomes

$$A(v)B^e(p) = \frac{1}{6} \sum_{g \in \mathbf{G}} \sum_{h_1 h_2 h_3 h_4 = e} T_+^{h_1} \otimes T_-^{h_2} \otimes T_+^{h_3 g^{-1}} L_+^g \otimes T_+^{g h_4} L_+^g \otimes L_-^g \otimes L_-^g. \quad (\text{D6})$$

Introducing the relabelling $h'_1 = h_1$, $h'_2 = h_2$, $h'_3 = h_3 g^{-1}$ and $h'_4 = g h_4$, we note that this set of new variables retains the initial condition $h'_1 h'_2 h'_3 h'_4 = h_1 h_2 h_3 g^{-1} g h_4 =$

$h_1 h_2 h_3 h_4 = e$ such that

$$A(v)B^e(p) = \frac{1}{6} \sum_{g \in \mathbf{G}} \sum_{h'_1 h'_2 h'_3 h'_4 = e} T_+^{h'_1} \otimes T_-^{h'_2} \otimes T_+^{h'_3} L_+^g \otimes T_+^{h'_4} L_+^g \otimes L_-^g \otimes L_-^g. \quad (\text{D7})$$

In this way each term in (D7) exactly matches one in (D3) and the commutativity condition $[A(v), B^e(p)] = 0$ is fulfilled. Crucially, for this and all other pairs of overlapping vertex and plaquette operators, this commutativity is ensured by choosing an orientation convention for the L_\pm^g and T_\pm^h operators such that one pair of L_\pm^g and T_\pm^h acting on the same qudit have the matching parity and the other have opposite parity. This ensures the condition $h'_1 h'_2 h'_3 h'_4 = e$ such that the two operators commute.

Similarly, for overlapping vertex (plaquette) operators, the L_\pm^g (T_\pm^h) operators acting on the single qudit point of overlap necessarily have opposite parity. For example, for the general case of two neighbouring vertex operators $A(v_i)$ and $A(v_j)$

$$[A(v_i), A(v_j)] \propto \sum_g \sum_h [L_\pm^g, L_\mp^h] = 0. \quad (\text{D8})$$

Appendix E: R matrix from ribbon operators

In Section III B we have shown how the exchange matrix $(R^{GG})^2$, describing the braiding of two G anyons, may be reproduced with projective measurements onto states constructed by exchanging the order of the ribbon operators $F_{\rho_1}^G$ and $F_{\rho_2}^G$, replicating Equation 13. This result may also be verified with direct evaluation of the operator products $F_{\rho_1}^G F_{\rho_2}^G$ and $F_{\rho_2}^G F_{\rho_1}^G$ in the basis $\{e, c, c^2, t, tc, tc^2\}$. By comparing the form of each operator, the R matrix can then be determined in the anyonic basis $\{A, B, G\}$. Such an approach can be experimentally relevant when quantum operator tomography is available.

By representing the ribbons operators $F_{\rho_1}^G$ and $F_{\rho_2}^G$ fully in terms of their elements of the isolated two lattice sites they cross over, we can find all the elements of the crossed terms

$$\begin{aligned}
F_{\rho_1}^G F_{\rho_2}^G &= \left((T_-^e + \omega T_-^c + \bar{\omega} T_-^{c^2}) \otimes L_-^c + (T_-^e + \bar{\omega} T_-^c + \omega T_-^{c^2}) \otimes L_-^{c^2} \right) \\
&\quad \times \left(L_+^c \otimes (T_-^e + \omega T_-^c + \bar{\omega} T_-^{c^2}) + L_+^{c^2} \otimes (T_-^e + \bar{\omega} T_-^c + \omega T_-^{c^2}) \right), \\
&= \left(\sum_h (|e\rangle \langle e| + \bar{\omega} |c\rangle \langle c| + \omega |c^2\rangle \langle c^2|) \otimes |c^2 h\rangle \langle h| + (|e\rangle \langle e| + \omega |c\rangle \langle c| + \bar{\omega} |c^2\rangle \langle c^2|) \otimes |ch\rangle \langle h| \right) \\
&\quad \times \left(\sum_g |gc\rangle \langle g| \otimes (|e\rangle \langle e| + \bar{\omega} |c\rangle \langle c| + \omega |c^2\rangle \langle c^2|) + |gc^2\rangle \langle g| \otimes (|e\rangle \langle e| + \omega |c\rangle \langle c| + \bar{\omega} |c^2\rangle \langle c^2|) \right), \\
&= |e, c^2\rangle \langle c, e| + |e, c^2\rangle \langle c^2, e| + |e, c\rangle \langle c, e| + |e, c\rangle \langle c^2, e| + \omega |c^2, c^2\rangle \langle e, e| + \omega |c^2, c^2\rangle \langle c, e| \\
&\quad + \bar{\omega} |c^2, c\rangle \langle e, e| + \bar{\omega} |c^2, c\rangle \langle c, e| + \bar{\omega} |c, c^2\rangle \langle e, e| + \bar{\omega} |c, c^2\rangle \langle c^2, e| + \omega |c, c\rangle \langle e, e| + \omega |c, c\rangle \langle c^2, e| \\
&\quad + \omega |e, e\rangle \langle c, c| + \bar{\omega} |e, e\rangle \langle c^2, c| + \omega |e, c^2\rangle \langle c, c| + \bar{\omega} |e, c^2\rangle \langle c^2, c| + \bar{\omega} |c^2, e\rangle \langle e, c| + |c^2, e\rangle \langle c, c| \\
&\quad + |c^2, c^2\rangle \langle e, c| + \omega |c^2, c^2\rangle \langle c, c| + \omega |c, e\rangle \langle e, c| + |c, e\rangle \langle c^2, c| + |c, c^2\rangle \langle e, c| + \bar{\omega} |c, c^2\rangle \langle c^2, c| \\
&\quad + \bar{\omega} |e, c\rangle \langle c, c^2| + \omega |e, c\rangle \langle c^2, c^2| + \bar{\omega} |e, e\rangle \langle c, c^2| + \omega |e, e\rangle \langle c^2, c^2| + |c^2, c\rangle \langle e, c^2| + \bar{\omega} |c^2, c\rangle \langle c, c^2| \\
&\quad + \omega |c^2, e\rangle \langle e, c^2| + |c^2, e\rangle \langle c, c^2| + |c, c\rangle \langle e, c^2| + \omega |c, c\rangle \langle c^2, c^2| + \bar{\omega} |c, e\rangle \langle e, c^2| + |c, e\rangle \langle c^2, c^2|,
\end{aligned} \tag{E1}$$

$$\begin{aligned}
F_{\rho_2}^G F_{\rho_1}^G &= \omega |e, c^2\rangle \langle c, e| + \bar{\omega} |e, c^2\rangle \langle c^2, e| + \bar{\omega} |e, c\rangle \langle c, e| + \omega |e, c\rangle \langle c^2, e| + \bar{\omega} |c^2, c^2\rangle \langle e, e| + |c^2, c^2\rangle \langle c, e| \\
&\quad + \omega |c^2, c\rangle \langle e, e| + |c^2, c\rangle \langle c, e| + \omega |c, c^2\rangle \langle e, e| + |c, c^2\rangle \langle c^2, e| + \bar{\omega} |c, c\rangle \langle e, e| + |c, c\rangle \langle c^2, e| \\
&\quad + \bar{\omega} |e, e\rangle \langle c, c| + \omega |e, e\rangle \langle c^2, c| + |e, c^2\rangle \langle c, c| + |e, c^2\rangle \langle c^2, c| + |c^2, e\rangle \langle e, c| + \bar{\omega} |c^2, e\rangle \langle c, c| \\
&\quad + \bar{\omega} |c^2, c^2\rangle \langle e, c| + \bar{\omega} |c^2, c^2\rangle \langle c, c| + |c, e\rangle \langle e, c| + \omega |c, e\rangle \langle c^2, c| + \omega |c, c^2\rangle \langle e, c| + \omega |c, c^2\rangle \langle c^2, c| \\
&\quad + |e, c\rangle \langle c, c^2| + |e, c\rangle \langle c^2, c^2| + |e, e\rangle \langle c, c^2| + \bar{\omega} |e, e\rangle \langle c^2, c^2| + \omega |c^2, c\rangle \langle e, c^2| + \omega |c^2, c\rangle \langle c, c^2| \\
&\quad + |c^2, e\rangle \langle e, c^2| + \omega |c^2, e\rangle \langle c, c^2| + \bar{\omega} |c, c\rangle \langle e, c^2| + \bar{\omega} |c, c\rangle \langle c^2, c^2| + |c, e\rangle \langle e, c^2| + \bar{\omega} |c, e\rangle \langle c^2, c^2|.
\end{aligned} \tag{E2}$$

Comparing these two expressions, we find that the elements of $F_{\rho_2}^G F_{\rho_1}^G$ gain an additional phase relative to those of $F_{\rho_1}^G F_{\rho_2}^G$ according to the following prescription

$$|g_1, g_2\rangle \langle h_1, h_2| \rightarrow \begin{cases} \bar{\omega} |g_1, g_2\rangle \langle h_1, h_2| & \text{if } g_1 g_2 = h_1 h_2 \\ \omega |g_1, g_2\rangle \langle h_1, h_2| & \text{otherwise.} \end{cases} \tag{E3}$$

To re-interpret this result into the anyonic basis as in (3), we consider the flux these ribbon operator products create on the shared plaquette, p . As the vacuum state is stabilised by the projector $B^e(p)$ it has trivial flux. As a result it consists of a superposition over all group elements for which $h_1 h_2 h_3 h_4 = e$ on that plaquette. Under the action of $|g_1, g_2\rangle \langle h_1, h_2|$, if $g_1 g_2 = h_1 h_2$, then the condition $g_1 g_2 h_3 h_4 = e$ is preserved. This condition corresponds to the fusion outcomes A and B that have trivial flux, that gain a factor $\bar{\omega}$, as seen from (E3). When $g_1 g_2 \neq h_1 h_2$, then $g_1 g_2 h_3 h_4 \neq e$ and the two ribbons have fused to produce a pair of G anyons with non-trivial flux. As seen from (E3), this fusion outcome acquires a phase factor ω as in the final diagonal element of (3).

Appendix F: Analytics for F matrix

We will now present the main calculations for the amplitudes that determine the elements of the F matrix squared. By taking the inner products of our ribbon fusion states as in (28), we find that for each combination $i, j = A, B, G$ a phase factor may be extracted,

$$\begin{aligned}
&\langle \psi_2(j) | \psi_1(i) \rangle \\
&= \langle \zeta | (A^G(v) F_{\rho_1}^G A^j(v) F_{\rho_2}^G F_{\rho_2}^G)^\dagger A^G(v) F_{\rho_2}^G A^i(v) F_{\rho_2}^G F_{\rho_1}^G | \zeta \rangle, \\
&= \langle \zeta | (F_{\rho_2}^G)^2 A^j(v) F_{\rho_1}^G A^G(v) F_{\rho_2}^G A^i(v) F_{\rho_2}^G F_{\rho_1}^G | \zeta \rangle, \\
&= \langle \zeta | F_{\rho_2}^j F_{\rho_1}^G A^G(v) A^G(v) F_{\rho_2}^G A^i(v) F_{\rho_2}^G F_{\rho_1}^G | \zeta \rangle, \\
&= (R_G^{Gj})^2 \langle \zeta | F_{\rho_1}^G F_{\rho_2}^j A^G(v) F_{\rho_2}^G A^i(v) F_{\rho_2}^G F_{\rho_1}^G | \zeta \rangle,
\end{aligned} \tag{F1}$$

where we have used the Hermiticity of each of our operators, $A^j(v) (F_{\rho_2}^G)^2 | \zeta \rangle = A^j(v) (F_{\tau_2}^A + F_{\tau_2}^B + F_{\rho_2}^G) | \zeta \rangle = F_{\tau/\rho_2}^j | \zeta \rangle$ and $A^G(v) F_{\rho_1}^G F_{\tau/\rho_2}^j | \zeta \rangle = \overline{(R_G^{Gj})}^2 A^G(v) F_{\tau/\rho_2}^j F_{\rho_1}^G | \zeta \rangle$. The string operator $F_{\tau_2}^j$ with $j = A$ or B is the direct triangle in the path ρ_2 , producing a pair of A or B anyons as in (C18) and (C19) respectively.

All these possible inner products can be reduced to phases and inner amplitudes with manipulations of the

ribbon operators. We see that if $j = A$ or B and $i = A, B$ or G , we can take

$$\begin{aligned}
& \langle \psi_2(j) | \psi_1(i) \rangle \\
&= (R_G^{Gj})^2 \langle \zeta | F_{\rho_1}^G F_{\rho_2}^j A^G(v) F_{\rho_2}^G A^i(v) F_{\rho_2}^G F_{\rho_1}^G | \zeta \rangle, \\
&= (R_G^{Gj})^2 \langle \zeta | F_{\rho_1}^G F_{\rho_2}^G A^i(v) A^i(v) F_{\rho_2}^G F_{\rho_1}^G | \zeta \rangle, \\
&= (R_G^{Gj})^2 \frac{1}{N_i^2} \langle \phi_{21}(i) | \phi_{21}(i) \rangle, \\
&= \frac{(R_G^{Gj})^2}{N_i^2},
\end{aligned} \tag{F2}$$

for the normalised states $|\phi_{21}(i)\rangle$ as defined in (15).

When $j = G$ and $i = A$ or B we have

$$\begin{aligned}
& \langle \psi_2(G) | \psi_1(i) \rangle \\
&= (R_G^{GG})^2 \langle \zeta | F_{\rho_1}^G F_{\rho_2}^G A^G(v) F_{\rho_2}^G A^i(v) F_{\rho_2}^G F_{\rho_1}^G | \zeta \rangle, \\
&= (R_G^{GG})^2 \langle \zeta | F_{\rho_1}^G (F_{\rho_2}^G)^2 A^i(v) F_{\rho_2}^G F_{\rho_1}^G | \zeta \rangle, \\
&= (R_G^{GG})^2 \langle \zeta | F_{\rho_1}^G F_{\rho_2}^G A^i(v) A^i(v) F_{\rho_2}^G F_{\rho_1}^G | \zeta \rangle, \\
&= \frac{(R_G^{GG})^2}{N_i^2}.
\end{aligned} \tag{F3}$$

And finally, for the case $i = j = G$

$$\begin{aligned}
& \langle \psi_2(G) | \psi_1(G) \rangle \\
&= (R_G^{GG})^2 \langle \zeta | F_{\rho_1}^G F_{\rho_2}^G A^G(v) F_{\rho_2}^G A^G(v) F_{\rho_2}^G F_{\rho_1}^G | \zeta \rangle, \\
&= \frac{(R_G^{GG})^2}{N_G^2} \langle \phi_{21}(G) | F_{\rho_2}^G | \phi_{21}(G) \rangle.
\end{aligned} \tag{F4}$$

The operator $F_{\rho_2}^G$ as defined in Eq. (C21) is constructed from terms of the form $L_+^g \otimes T_-^h$. The non-zero matrix elements of the operators T_-^h lie on the main diagonal, whereas L_+^g act as permutation operators between group elements such that the resultant operator $F_{\rho_2}^G$ is traceless and we obtain the required $\langle \psi_2(G) | \psi_1(G) \rangle = 0$.

These analytical values for each of the overlaps $\langle \psi_2(j) | \psi_1(i) \rangle$ may be substituted into Equation (29) in order to determine each of the values of the F matrix squared.

Appendix G: Derivation of the 2 Qudit Groundstate

The derivation of R and \mathcal{F} may be represented as the calculation of overlaps of the form

$$\langle \eta | O_{a,4}^\dagger O_{b,4} | \eta \rangle, \tag{G1}$$

where $O_{i,4}$ indicates a matrix acting on the 6^4 -dimensional Hilbert space of a single plaquette and $|\eta\rangle$ is the ground state of the Kitaev Hamiltonian on this system

$$\mathcal{H}_4 = -B(p) - \sum_{i=1}^4 A(v_i), \tag{G2}$$

where the vertex operators, $A(v_i)$, act non-trivially on only two qudits, such that for example

$$A(v_3) = \frac{1}{6} \sum_{g \in \mathbf{G}} \mathbf{1}_6 \otimes \mathbf{1}_6 \otimes L_+^g \otimes L_-^g. \tag{G3}$$

. We have also shown, however, that each operator acting on $|\eta\rangle$ in the states (36) and (37), only acts non-trivially on qudits 3 and 4. We may therefore rewrite

$$\langle \eta | O_{a,4}^\dagger O_{b,4} | \eta \rangle = \langle \eta | (\mathbf{1}_{36} \otimes O_a^\dagger) (\mathbf{1}_{36} \otimes O_b) | \eta \rangle \tag{G4}$$

$$= \langle \eta | (\mathbf{1}_{36} \otimes O_a^\dagger O_b) | \eta \rangle \tag{G5}$$

$$= \langle \eta | \begin{pmatrix} O_a^\dagger O_b & 0 & \dots & 0 \\ 0 & O_a^\dagger O_b & \dots & 0 \\ \vdots & \vdots & \ddots & \vdots \\ 0 & 0 & \dots & O_a^\dagger O_b \end{pmatrix} | \eta \rangle. \tag{G6}$$

Each element ' $O_a^\dagger O_b$ ' is itself a 36×36 matrix, such that this expression may be further simplified by decomposing $|\eta\rangle$ into a set of 36-dimensional vectors. It is found that $|\eta\rangle$ may be written in the following form

$$|\eta\rangle = \begin{pmatrix} |\psi_1\rangle \\ |\psi_2\rangle \\ |\psi_3\rangle \\ |\psi_4\rangle \\ |\psi_5\rangle \\ |\psi_6\rangle \end{pmatrix} = \begin{pmatrix} |\psi_1\rangle \\ (L_-^c \otimes \mathbf{1}_{36}) |\psi_1\rangle \\ (L_-^{c^2} \otimes \mathbf{1}_{36}) |\psi_1\rangle \\ (L_-^t \otimes \mathbf{1}_{36}) |\psi_1\rangle \\ (L_-^{tc} \otimes \mathbf{1}_{36}) |\psi_1\rangle \\ (L_-^{tc^2} \otimes \mathbf{1}_{36}) |\psi_1\rangle \end{pmatrix}, \tag{G7}$$

where $|\psi_1\rangle$ is a 6^3 -dimensional vector of the form

$$|\psi_1\rangle = \begin{pmatrix} |\psi_e\rangle \\ |\psi_c\rangle \\ |\psi_{c^2}\rangle \\ |\psi_t\rangle \\ |\psi_{tc}\rangle \\ |\psi_{tc^2}\rangle \end{pmatrix}, \quad |\psi_g\rangle = \frac{1}{\sqrt{216}} \sum_{g_1 g_2 = g} |g_1, g_2\rangle. \tag{G8}$$

These $|\psi_g\rangle$ are the 36-dimensional vectors on which $O_a^\dagger O_b$ will act.

The single-qudit right multiplication operators L_-^g are essentially permutation operators such that, for example

$$|\psi_2\rangle = (L_-^c \otimes \mathbf{1}_{36}) |\psi_1\rangle = \begin{pmatrix} |\psi_c\rangle \\ |\psi_{c^2}\rangle \\ |\psi_e\rangle \\ |\psi_{tc}\rangle \\ |\psi_{tc^2}\rangle \\ |\psi_t\rangle \end{pmatrix}. \tag{G9}$$

We therefore see that each 36-dimensional vector $|\psi_g\rangle$ will appear in each of $|\psi_1\rangle, |\psi_2\rangle, \dots, |\psi_6\rangle$ once and therefore in total in $|\eta\rangle$ six times.

Our inner product terms may thus be expanded as the sum of six terms

$$\langle \eta | (\mathbf{1}_{36} \otimes O_a^\dagger O_b) | \eta \rangle = 6 \sum_{g \in G} \langle \psi_g | O_a^\dagger O_b | \psi_g \rangle. \quad (\text{G10})$$

The summation over $g \in G$ of $|\psi_g\rangle$ means that we are actually considering the action of $O_a^\dagger O_b$ on every state of our system. We may therefore equivalently compute the overlap as the innerproduct of $O_a^\dagger O_b$ on a single vector

$$\langle \eta | (\mathbf{1}_{36} \otimes O_a^\dagger O_b) | \eta \rangle = 6 \cdot \langle \xi | O_a^\dagger O_b | \xi \rangle, \quad (\text{G11})$$

where

$$|\xi\rangle = \frac{1}{\sqrt{216}} \sum_{g_3, g_4 \in G} |g_3, g_4\rangle. \quad (\text{G12})$$

Finally, we note that this calculation is also equivalent to simply summing every element in the product matrix $O_a^\dagger O_b$

$$6 \cdot \langle \xi | O_a^\dagger O_b | \xi \rangle = \frac{1}{36} \sum_{g_3, g_4 \in G} \langle g_3, g_4 | O_a^\dagger O_b | g_3, g_4 \rangle \quad (\text{G13})$$

$$= \frac{1}{36} \sum_{i, j=1}^{36} [O_a^\dagger O_b]_j^i \quad (\text{G14})$$

circumventing the need for state preparation and thus providing another alternative experimental implementation if quantum operator tomography is available.